https://doi.org/10.5194/egusphere-2026-2804
Preprint. Discussion started: 28 July 2026

Implementation of an eco-evolutionary approach to photosynthesis and acclimation in the JULES land surface model

Wenyao Gan[1], Martin Best[2], Pier Luigi Vidale[3] , I. Colin Prentice[4] and Sandy P. Harrison[1]

1: Department of Geography and Environmental Science, University of Reading, Reading, RG6 6AB, UK

2: Meteorological Office, Fitzroy Road, Exeter, EX1 3PB, UK

3: Department of Meteorology, University of Reading, Reading, RG6 6AB, UK

4: Department of Life Sciences, Georgina Mace Centre for the Living Planet, Imperial College London, Silwood Park Campus, Buckhurst Road, Ascot, SL5 7PY, UK

Correspondence: Wenyao Gan w.gan@pgr.reading.ac.uk

Abstract. Realistic simulation of photosynthesis is needed for accurate prediction of the global carbon cycle. In addition to the well-known instantaneous response to changes in temperature, photosynthetic processes acclimate to long-term environmental changes by adjusting the maximum photosynthetic capacities (V_{cmax} and J_{max}) and stomatal behaviour The theoretical basis for acclimation can be understood as an outcome of eco-evolutionary optimality (EEO). Here, we have implemented an EEO-based scheme to represent the universal acclimation of photosynthesis to environmental conditions independently of plant functional types in the JULES land surface model. We compare this implementation with two standard configurations of JULES (GL7, UKESM1). We evaluate model performance using daily, monthly and annual site-based observations of gross primary production (GPP) observations at flux towers from the PLUMBER2 data set. The EEO-based scheme, PJULES, produces better predictions of GPP than either GL7 or UKESM1, both of which substantially underestimate GPP at the higher end of the observed range. Comparison at individual sites shows that PJULES produces more realistic simulations of seasonal and diurnal cycles of GPP. The improvement in the estimation of GPP does not degrade simulated land-surface energy fluxes: predictions of the latent heat flux are similar to those from the UKESM1 and slightly better than those from GL7. The good performance of PJULES shows that a parsimonious model can offer a competitive alternative to more complex parameterisations for simulating land–atmosphere carbon and water exchanges.

https://doi.org/10.5194/egusphere-2026-2804
Preprint. Discussion started: 28 July 2026

1. Introduction

The land surface plays a critical role in the global climate system, functioning as a carbon sink that currently removes about one-third of the total anthropogenic emissions and thereby slowing the rate of climate change (Friedlingstein et al., 2025; Ruehr et al., 2023). The total amount of carbon fixed through photosynthesis, quantified as gross primary production (GPP), is the dominant flux in the terrestrial carbon cycle and represents a global uptake of approximately 120–150 Pg C yr^{-1} (Anav et al., 2015; Beer et al., 2010; Friedlingstein et al., 2025; Jiang and Ryu, 2016). The ability to model GPP realistically is important for quantifying the magnitude and variability of the land carbon sink and its feedback to the climate system (Campbell et al., 2017; Rogers et al., 2017; Ruehr et al., 2023)

Land surface models (LSMs) simulate the exchanges of carbon, water, and energy between the land surface and the atmosphere, and are therefore a key component of weather, seasonal, climate and Earth System Models (ESMs) used for environmental prediction (Fisher and Koven, 2020; Lawrence et al., 2019). Most LSMs prescribe key physiological traits that control photosynthesis, including the maximum carboxylation rate (V_{cmax}) and maximum electron transport rate (J_{max}) at standard temperature, as constant parameters that vary between but not within plant functional types (PFTs). Furthermore, different LSMs use varying numbers and definitions of PFTs, each with its own model-specific calibration. These differences in model structure contribute to systematic mismatches in model predictions and disagreements with observations (Canadell et al., 2021).

In addition to the instantaneous response of photosynthetic parameters to temperature, experimental and observational evidence has demonstrated that photosynthetic capacity acclimates to growth temperature on a time scale of days to weeks (Carter et al., 2021; Crous, 2019; Drake et al., 2015; Dusenge et al., 2020; Reich et al., 2018), leading to systematic shifts in both the magnitude and temperature optimum of carbon assimilation (Kumarathunge et al., 2019; Way and Yamori, 2014; Yamori et al., 2013). Standardised V_{cmax} ($V_{cmax,25}$) declines under sustained thermal stress (Scafaro et al., 2017), and the ratio of $J_{max,25}$ to $V_{cmax,25}$ adjusts dynamically in response to prevailing temperatures (Smith and Dukes, 2017). These findings highlight a fundamental limitation of the PFT-based parameterisation approach: fixed photosynthetic parameters do not capture these physiological responses to environmental change.

https://doi.org/10.5194/egusphere-2026-2804
Preprint. Discussion started: 28 July 2026

Some LSMs have included representations of photosynthetic temperature acclimation using an empirical scheme developed by Kattge and Knorr (2007) and updated by Kumarathunge et al. (2019). Both of these schemes have been implemented in the Joint UK Land Environment Simulator (JULES), the LSM used in the UK Earth System Model (UKESM). Implementation of the Kattge and Knorr (2007) scheme in JULES resulted in improvements in simulated GPP and evapotranspiration under current climate, particularly in tropical regions, in high-latitude northern hemisphere forests during summer, and in temperate and boreal evapotranspiration across the northern hemisphere (Oliver et al., 2022). However, the empirical algorithms from Kattge and Knorr (2007) were based on a limited data set, particularly lack in tropical biomes. The Kumarathunge et al. (2019) scheme is based on a larger data set and has improved tropical coverage. Incorporation of this scheme to represent thermal acclimation in JULES produced a further improvement in the simulation of GPP (Oliver et al., 2025). Nevertheless, while these empirical schemes improve model flexibility compared to fixed-parameter approaches, they still use PFT-specific parameterisations, and they do not provide a unified explanation for why plants adjust their thermal responses in the ways observed experimentally.

Acclimation is not represented in the two of the most widely used JULES configurations: GL7 (Wiltshire et al., 2020) and UKESM1 (Sellar et al., 2019). Both configurations employ the Collatz model (Collatz et al., 1991) with fixed PFT-dependent photosynthetic parameters. The UKESM1 configuration extends GL7 by expanding from five to thirteen PFTs and incorporating additional processes including a representation of nitrogen limitation (Wiltshire et al., 2021) and updated representations of plant physiology (Harper et al., 2018), but still retains the underlying static parameterisation of photosynthetic capacity.

The limitations of both the standard configurations and the empirical acclimation schemes previously implemented in JULES highlight the need for an alternative approach that can represent photosynthetic responses to environmental change without relying on PFT-specific parameterisations or empirical relationships. Eco-evolutionary optimality (EEO) based approaches have been advocated as a way of providing robust, parameter-sparse models of plant and vegetation processes (Harrison et al., 2021). Here, we test this by implementing an EEO-based scheme for gross primary production, the P-model, in JULES. The original P-model predicts photosynthetic traits directly from environmental drivers at weekly to monthly timesteps (Prentice et al., 2014; Stocker et al., 2020; Wang et al., 2017). However, there is a sub-daily formulation which explicitly separates the instantaneous (sub-daily) and acclimated

https://doi.org/10.5194/egusphere-2026-2804
Preprint. Discussion started: 28 July 2026

responses to environmental drivers and was designed for implementation in LSMs (Mengoli et al., 2022). In this study, implement this sub-daily version in JULES and evaluate the performance of the new scheme (PJULES) in predicting observed GPP and latent heat (LE) from eddy-covariance flux sites against the two standard JULES configurations at annual and monthly timescales, and over seasonal and diurnal cycles. We also perform sensitivity analyses to identify the causes of differences between the three model configurations.

2 Model description

2.1 JULES land surface model

JULES (Best et al., 2011; Clark et al., 2011) is the land surface model used by the UK weather and climate modelling community. JULES simulates the exchange of radiation, heat, water, momentum, and carbon between the land surface and the atmosphere, and represents sub-grid heterogeneity through a tiling approach in which each surface type maintains its own energy budget coupled to a shared soil column. Soil processes are represented using a four-layer scheme (0.1, 0.25, 0.65, and 2.0 m thick) with hydraulic relationships following Van Genuchten (1980) and sub-grid soil moisture heterogeneity optionally parameterised using TOPMODEL (Gedney and Cox, 2003). Leaf-level stomatal conductance and photosynthesis are coupled through CO_2 diffusion (Cox et al., 1998), with canopy-level scaling achieved via a 10-layer canopy radiation model using the two-stream approach of Sellers (1985). Surface exchange follows Monin-Obukhov similarity theory of Beljaars and Holtslag (1991) under stable conditions and the Dyer (1974) forms under unstable conditions. A multilayer snow scheme with up to three layers is used incorporating prognostic thickness, water content, temperature, and grain size, with snow thermal conductivity following Calonne et al. (2011).

2.2 JULES Model configurations

The two standard configurations of JULES are JULES-GL7 (Wiltshire et al., 2020) and JULES-UKESM1 (Sellar et al., 2019). The first configuration follows the JULES Global Land 7 (JULES-GL7; Wiltshire et al., 2020), the standard global land configuration used in the sixth phase of the Coupled Model Intercomparison Project (CMIP6) as part of HadGEM3-GC3.1 (Williams et al., 2018) and implemented here using JULES vn7.0. JULES-GL7 represents the land surface using five PFTs (broadleaf trees, needleleaf trees, C_3 grass, C_4 grass, and shrubs)

https://doi.org/10.5194/egusphere-2026-2804
Preprint. Discussion started: 28 July 2026

and four non-vegetated surface types (urban, inland water, bare soil, and ice). Each PFT has different parameter values governing photosynthesis, stomatal conductance, root distribution, canopy structure, and radiative properties (Tables 1 and 2 in Wiltshire et al., 2020).

The second configuration uses the JULES setup implemented in UKESM1 (Sellar et al., 2019), the UK Earth System Model used in CMIP6, implemented here using JULES vn7.8. This configuration extends the 5-PFT scheme to 13 PFTs, subdividing broadleaf trees into broadleaf deciduous, broadleaf evergreen temperate, and broadleaf evergreen tropical types, needleleaf trees into needleleaf deciduous and needleleaf evergreen, shrubs into deciduous and evergreen shrub types, C_3 grassland into C_3 natural grass, C_3 crop, and C_3 pasture, and C_4 grassland into C_4 natural grass, C_4 crop, and C_4 pasture (Harper et al., 2016, 2018). The expanded PFT scheme provides a more refined representation of plant physiological diversity allowing, for example, tropical and temperate broadleaf evergreen PFTs to have different photosynthetic temperature responses (Table 1). The UKESM1 Earth system configuration includes interactive dynamic vegetation via TRIFFID (Cox, 2001), coupled carbon–nitrogen cycling (Wiltshire et al., 2021), and a representation of land use changes (Burton et al., 2019), but these components are disabled in this study to maintain consistency with the offline experimental design used for the GL7 simulations; phenology is prescribed from satellite-derived LAI in all three configurations evaluated here. JULES configurations are designed to be independent of the underlying code version, with different code releases producing the same results for a given configuration (Wiltshire et al., 2020). The use of different JULES code versions (vn7.0 and vn7.8) therefore does not introduce scientific differences. The principal difference between the two configurations is the number of PFTs and the associated parameter sets governing the physiological and radiative properties of vegetation.

2.2.1 Photosynthesis in JULES

Leaf-level photosynthesis for C_3 plants in JULES follows the approach of Collatz et al. (1991), where the net photosynthesis rate is determined by the most limiting of three potential rates: the light-limited rate (W_l) which depends on the quantum efficiency (α), the Rubisco-limited rate (W_c), and the rate limited by transport of photosynthetic products (W_e) (see Note S1 for detailed description of the calculation of these three limiting rates). Both W_c and W_e depend on V_{cmax}, the maximum rate of Rubisco carboxylation, which is derived from V_{cmax} standardised at 25°C ($V_{cmax,25}$), scaled by a temperature response function:

$$V_{\mathrm{cmax}} = V_{\mathrm{cmax},25} \cdot \frac{f_T(T_C)}{\left[1+\exp\left(0.3(T_C - T_{\mathrm{upp}})\right)\right]\left[1+\exp\left(0.3(T_{\mathrm{low}} - T_C)\right)\right]} \quad \text{Eqn.1}$$

https://doi.org/10.5194/egusphere-2026-2804
Preprint. Discussion started: 28 July 2026

where T_C is canopy temperature (°C), T_{upp} and T_{low} are PFT-dependent upper and lower temperature limits for photosynthesis, and

$$f_T(T_C) = Q_{10,leaf}^{0.1(T_C-25)} \quad \text{Eqn.2}$$

with $Q_{10,leaf} = 2.0$.

The multi-layer canopy scheme (can_rad_mod = 6; Clark et al., 2011) explicitly resolves sunlit and shaded leaves within each of 10 canopy layers, with two-stream radiation transfer and sunfleck penetration. Sunfleck penetration through the canopy is parameterised as:

$$f_{sun} = \exp\left(-\frac{k_b}{\cos z} \cdot LAI\right) \quad \text{Eqn.3}$$

where k_b= 0.5 and z is the solar zenith angle. The leaf scattering coefficient for PAR (ω) governs the attenuation of radiation through the canopy via the two-stream radiative transfer scheme, influencing the photosynthetically active radiation (PAR) available to sunlit and shaded leaves in each canopy layer. Leaf nitrogen is assumed to decay exponentially as a function of cumulative leaf area index, with a nitrogen decay coefficient k_n = 0.2 (Wiltshire et al., 2020), such that $V_{cmax,25}$ at canopy depth L is:

$$V_{cmax,25}(L) = n_{eff} \cdot n_{l0} \cdot \exp(-k_n \cdot L) \quad \text{Eqn.4}$$

Parameters governing leaf-level photosynthesis for both the JULES-GL7 and JULES-UKESM1 configurations are defined for each PFT (Table 1). Leaf photosynthesis is calculated as:

$$A_l = W \cdot \beta \quad \text{Eqn.5}$$

where A_l is the leaf-level gross photosynthesis, W is the smoothed minimum of the three limiting rates (W_l, W_c and W_e) and β is a soil moisture stress factor (Eqn.S10). The factor β is 1 when the soil moisture content of the root zone ($\theta: m^3\ m^{-3}$) is at or above a critical threshold (θ_{crit}), which depends on soil texture. When soil water content drops below θ_{crit}, β decreases linearly until θ reaches the wilting point (where β = 0) (Best et al., 2011). Leaf-level photosynthesis is calculated separately for sunlit and shaded leaves at each of the 10 canopy layers, with sunlit leaves receiving both direct and diffuse radiation and shaded leaves receiving only diffuse radiation. Total canopy GPP is then obtained by integrating over all sunlit and shaded leaf fractions across the 10 layers.

https://doi.org/10.5194/egusphere-2026-2804
Preprint. Discussion started: 28 July 2026

Table 1. Comparison of values for key photosynthesis parameters across different plant functional types in the two standard JULES configurations. In JULES-GL7 , these are broadleaf tree (BT), needleleaf tree (NT), C_3 grass and shrub In JULES-UKESM1, these are broadleaf deciduous tree (BDT), broadleaf evergreen tropical tree (BET-Tr), broadleaf evergreen temperate tree (BER-Te), needleleaf deciduous tree (NDT) and needleleaf evergreen tree (NET), C_3 natural grass, C_3 crop, C_3 pasture, C_4 grassland into C_4 natural grass, C_4 crop, C_4 pasture, deciduous shrub (DSH) and evergreen shrub (ESH). The parameters are the extinction coefficient for photosynthetically active radiation, PAR (*kpar*), quantum efficiency (mol CO_2 per mol PAR photons) (α), the leaf scattering coefficient for PAR (Ω), the top leaf nitrogen concentration, kg N/kg C (n_{l0}), the lower temperature for photosynthesis (T_{low}), the upper temperature for photosynthesis (T_{upp}), and the scale factor relating V_{cmax} with leaf nitrogen concentration (n_{eff}).

GL7	UKESM1	*kpar*	α	Ω	n_{l0}	T_{low}	T_{upp}	n_{eff}
BT		0.5	0.08	0.15	0.04	0	36	0.0008
	BDT	0.5	0.064	0.105	0.046	10	43	0.0008
	BET-Tr	0.5	0.064	0.104	0.046	13	43	0.0008
	BET-Te	0.5	0.048	0.058	0.046	13	43	0.0008
NT		0.5	0.08	0.15	0.03	−10	31	0.0008
	NDT	0.5	0.08	0.083	0.033	−10	26	0.0008
	NET	0.5	0.064	0.083	0.033	0	32	0.0008
C_3 grass		0.5	0.08	0.15	0.06	0	36	0.0008
	C_3 natural grass	0.5	0.048	0.116	0.073	10	32	0.0008
	C_3 crop	0.5	0.048	0.125	0.073	10	32	0.0008
	C_3 pasture	0.5	0.048	0.116	0.073	10	32	0.0008
C_4 grass		0.5	0.04	0.17	0.03	13	45	0.0004
	C_4 natural grass	0.5	0.04	0.135	0.06	13	45	0.0004
	C_4 crop	0.5	0.04	0.136	0.06	13	45	0.0004
	C_4 pasture	0.5	0.04	0.135	0.06	13	45	0.0004
Shrub		0.5	0.08	0.15	0.03	0	36	0.0008
	DSH	0.5	0.064	0.125	0.06	10	40	0.0008
	ESH	0.5	0.048	0.073	0.06	0	36	0.0008

https://doi.org/10.5194/egusphere-2026-2804
Preprint. Discussion started: 28 July 2026

2.2.2 Stomatal conductance in JULES

Stomatal conductance (g_s) in JULES is coupled to photosynthesis through the leaf internal concentration of CO_2 (c_i). In both JULES-GL7 and JULES-UKESM1, c_i is calculated using the Jacobs scheme (Best et al., 2011; Jacobs, 1994):

$$c_i = (c_a - \Gamma^*) \cdot f_0 \cdot \left(1 - \frac{d_q}{dq_{crit}}\right) + \Gamma^* \quad \text{Eqn.6}$$

where c_a is the ambient CO_2 partial pressure (Pa), Γ* is the CO_2 compensation point in the absence of mitochondrial respiration (Pa), d_q is the specific humidity deficit at the leaf surface (kg kg^{-1}), and f_0 (dimensionless) and d_{qcrit} (kg kg^{-1}) are PFT-specific parameters representing the ci/ca ratio at zero humidity deficit and the critical humidity deficit at which stomata close, respectively.

g_s is then derived from c_i and the net assimilation rate via Fick's law of diffusion (von Caemmerer and Farquhar, 1981):

$$g_s = \frac{1.6 \cdot R \cdot T_l \cdot A_n}{c_a - c_i} \quad \text{Eqn.7}$$

where the factor 1.6 accounts for the ratio of diffusivities of water vapour and CO_2 in air, R is the universal gas constant, and T_l is the leaf temperature (K). The Jacobs scheme implies a linear decrease in c_i/c_a with increasing humidity deficit, with stomata fully closing when $d_q \geq d_{qcrit}$ or when the soil moisture stress factor β = 0.

2.3 PJULES

2.3.1 Photosynthesis

PJULES is developed on the basis of JULES vn7.0, replacing the multilayer Collatz et al. (1991) leaf-level photosynthesis and the Jacobs stomatal conductance scheme by the big-leaf P-model (Prentice et al., 2014; Wang et al., 2017; Mengoli et al., 2022) (can rad mod = 1, photo model = 3). The P-model is based on the Farquhar et al. (1980) biochemical model of C_3 photosynthesis, in which the instantaneous assimilation rate A is determined by the lesser of the Rubisco-limited rate of carboxylation (A_c), which depends on the maximum rate of V_{cmax} and the effective Michaelis-Menten coefficient (K_{mm}), and the electron transport-limited rate A_J, which depends on the quantum efficiency (φ_0) and J_{max}. Unlike the Collatz et al. (1991)

https://doi.org/10.5194/egusphere-2026-2804
Preprint. Discussion started: 28 July 2026

model, the P-model does not include *We* and determines A as the strict minimum of A_c and A_J rather than a smoothed co-limitation.

V_{cmax} and J_{max} are predicted from the coordination hypothesis (Haxeltine and Prentice, 1996; Maire et al., 2012) determined by environmental conditions rather than prescribed as PFT-specific parameters.

$$V_{cmax} = \frac{\varphi_0 I_{abs}[(c_i + K_{mm})}{(c_i + 2\Gamma^*)} \sqrt{\left\{1 - \left[c^* \frac{(c_i+2\Gamma^*)}{(c_i-\Gamma^*)}\right]^{\frac{2}{3}}\right\}} \quad \text{Eqn.8}$$

$$J_{max} = \frac{4\varphi_0 I_{abs}}{\sqrt{\frac{1}{\left\{1 - \left[c^* \frac{(c_i+2\Gamma^*)}{(c_i-\Gamma^*)}\right]^{\frac{2}{3}}\right\}} - 1}} \quad \text{Eqn.9}$$

where φ_0 is the intrinsic quantum yield of photosynthesis (mol CO_2 mol^{-1} photons), $\Gamma^*$is the temperature-dependent CO_2 compensation point (Pa), I_{abs} = fAPAR × PPFD, PPFD is incident photosynthetic photon flux density and fAPAR is the fraction of absorbed photosynthetically active radiation derived from satellite observed leaf area index (LAI) using Beer's law (Beer et al., 2010): fAPAR=1-exp(-k·LAI). k = 0.5 is the light extinction coefficient. c^* is a cost parameter (0.41) for electron transport capacity (Wang et al., 2017).

2.3.2 Stomatal conductance

The least-cost hypothesis (Prentice et al., 2014; Wright et al., 2003) predicts the optimal χ ($\chi = c_i/c_a$) by minimising the combined costs of maintaining carboxylation capacity and transpiration (stomate model = 3), replacing the Jacobs scheme described in Sect. 2.2. The optimal intercellular CO_2 partial pressure is then:

$$c_i = \chi \times c_a = \frac{\xi C_a + \Gamma^* \sqrt{VPD}}{\xi + \sqrt{VPD}} \quad \text{Eqn.10}$$

where c_a is the ambient atmospheric CO_2 partial pressure (Pa) and VPD is the vapour pressure deficit (Pa), Γ^* is the temperature-dependent CO_2 compensation point (Pa), and ξ is the optimal stomatal sensitivity.

https://doi.org/10.5194/egusphere-2026-2804
Preprint. Discussion started: 28 July 2026

2.3.3 Acclimation scheme

PJULES incorporates the acclimation scheme from the sub-daily P-model (Mengoli et al., 2022), which extends the standard P-model framework by explicitly distinguishing between instantaneous and acclimated photosynthetic responses. V_{cmax25}, J_{max25} and ξ are determined at the acclimation timescale. Daily optimal acclimation targets ($V^{(d)}_{cmax,opt}$, $J^{(d)}_{max,opt}$, $\xi^{(d)}_{opt}$) are determined from conditions during a midday window (11:30-12:30 local solar time), when PPFD is highest, and the coordination hypothesis is applied.

Daily optimal values are normalised to a 25 °C reference temperature

$$V^{(d)}_{cmax25,opt} = V^{(d)}_{cmax,opt}/f_V(T_{noon}) \quad \text{Eqn.11}$$

$$J^{(d)}_{max25,opt} = J^{(d)}_{max,opt}/f_J(T_{noon}) \quad \text{Eqn.12}$$

The temperature response of both quantities follows the basic Arrhenius function:

$$f(T) = \exp\left[\frac{\Delta Ha}{R}\left(\frac{1}{298.15} - \frac{1}{T}\right)\right] \quad \text{Eqn.13}$$

where ΔH_a is the activation energy (65,330 J mol^{-1} for V_{cmax} (Bernacchi et al., 2001) and 43,900 J mol^{-1} for J_{max} (Bernacchi et al., 2003), R is the universal gas constant (8.314 J mol^{-1} K^{-1}), and T is the surface temperature (K).

The acclimated parameters are smoothed using a weighted running mean with a 15-day memory (α = 1/15):

$$\bar{V}^{(d)}_{cmax25} = \alpha\bar{V}^{(d)}_{cmax25} + (1-\alpha)V^{(d-1)}_{cmax25,opt} \quad \text{Eqn.14}$$

$$\bar{J}^{(d)}_{max25} = \alpha\bar{J}^{(d)}_{max25} + (1-\alpha)J^{(d-1)}_{max25,opt} \quad \text{Eqn.15}$$

$$\bar{\xi}^{(d)} = \alpha\bar{\xi}^{(d)} + (1-\alpha)\xi^{(d-1)}_{opt} \quad \text{Eqn.16}$$

These acclimated values are updated once daily (at 12:30 pm local time) and held constant within each day. To obtain the instantaneous photosynthetic capacities, they are rescaled to the current temperature *T(t)* via the Arrhenius function:

$$V_{cmax}(t) = \bar{V}^{(d)}_{cmax25} \cdot f_V\big(T(t)\big) \quad \text{Eqn.17}$$

https://doi.org/10.5194/egusphere-2026-2804
Preprint. Discussion started: 28 July 2026

$$J_{\max}(t) = \bar{J}^{(d)}_{\max 25} \cdot f_J\big(T(t)\big) \quad \text{Eqn.18}$$

The instantaneous $c_i(t)$ is computed from slowly acclimating $\bar{\xi}^{(d)}$ together with instantaneous VPD:

$$c_i(t) = \frac{\xi_d \cdot c_a(t) + \Gamma^*(T(t)) \cdot \sqrt{\mathrm{VPD}(t)}}{\xi_d + \sqrt{VPD(t)}} \quad \text{Eqn.19}$$

The $A_c(t)$ and $A_J(t)$ are calculated:

$$A_c(t) = V_{\mathrm{cmax}}(t)\frac{c_i(t) - \Gamma^*(t)}{c_i(t) + K_{\mathrm{mm}}(t)} \quad A_J(t) = J(t)\frac{c_i(t) - \Gamma^*(t)}{c_i(t) + 2\Gamma^*(t)} \quad \text{Eqn.20}$$

Canopy-level GPP is obtained by applying the big-leaf approach:

$$\mathrm{GPP}(t) = \mathrm{fAPAR} \cdot minn\left(A_{\mathrm{c}}(t), A_{\mathrm{J}}(t)\right) \cdot \beta \quad \text{Eqn.21}$$

A full description of the sub-daily P model is provided in Note S2. All other aspects of the land surface model, including the algorithm to predict β using the same piecewise linear function (see Eq. S10), are unchanged. Table 2 provides a summary of the key structural differences between the three model configurations.

Table 2. Description of the three model configurations evaluated in this study.

	GL7	**UKESM1**	**PJULES**
JULES version	vn7.0	vn7.8	vn7.0
Number of PFTs	5	13	2
Photosynthesis scheme	Collatz	Collatz	P model
Temperature response of V_{cmax}	Q_{10}	Q_{10}	Arrhenius
V_{cmax25}	Prescribed	Prescribed	Predicted
J_{max}	Not defined	Not defined	Predicted
Stomatal conductance	Jacobs	Jacobs	Predicted
Canopy scheme	10 layers	10 layers	Big leaf
Acclimation	None	None	15-day exponential moving average
PFT-specific photosynthetic parameters	Yes	Yes	No
Soil moisture stress (β)	Piecewise linear	Piecewise linear	Piecewise linear

2.4 Data and evaluation

Model simulations were driven by quality-controlled and gap-filled meteorological forcing from the PLUMBER2 dataset (Ukkola et al., 2022), which compiles half-hourly observations from 170 eddy covariance sites drawn from the FLUXNET2015, La Thuile, and OzFlux collections. The forcing variables used include air temperature (T_air, °C), relative humidity

https://doi.org/10.5194/egusphere-2026-2804
Preprint. Discussion started: 28 July 2026

(RH, %), air pressure (Pa), and downwelling shortwave radiation (W m^{-2}). Peat bog, wetland, irrigated and C_4-dominated sites were excluded from the analysis, resulting in a final dataset of 130 sites spanning a wide range of climate zones and vegetation types. Site records covered from 1 to 21 years during the period 1992-2018 (Table S1). Sites with hourly data were resampled to half-hourly resolution within JULES. LAI was prescribed as an ancillary input derived from global satellite products available in PLUMBER2, including estimates from MODIS and the Copernicus Global Land Service. PFT fractions were derived from MODIS land cover products. The full 134-site dataset was used to evaluate model performance at monthly and annual timescales A subset of seven sites was used to assess the seasonal and diurnal cycles of simulated GPP and LE. These sites represent a range of climate and vegetation types (Table 3), including evergreen boreal forest (FI-Hyy), boreal mixed forest (RU-Fyo), temperate deciduous broadleaf forest (US-UMB), temperate mixed forest (BE-Vie), tropical forest (GF-Guy), temperate grassland (CH-Cha), and temperate managed grassland (DE-Gri). For the sub-daily timescale analysis, we used data from week 34 (21–27 August) in 2014 for these seven sites, for comparability with Mengoli et al. (2022). For the seasonal cycle analysis, the evaluation period was January 2011 to December 2014 for most sites, but only for 2011, 2012, and 2014 at US-UMB and 2007, 2009, 2013, and 2014 at GF-Guy because of data availability and quality.

Model performance at monthly and yearly time scales was evaluated against observed GPP derived using the nighttime partitioning method (GPP_NT_VUT_REF) and latent heat flux (LE_F_MDS). For the seven sites selected for seasonal and diurnal evaluation, observational uncertainty was characterised using the 5th and 95th percentile confidence interval of the nighttime partitioning estimate (GPP_NT_VUT_05 and GPP_NT_CUT_95). For LE, observational uncertainty was characterised using the 25th and 75th percentile estimates of the energy-balance-corrected latent heat flux (LE_CORR_25 and LE_CORR_75). These corrected estimates were not available for US-UMB, GF-Guy, and CH-Cha.

Model performance was evaluated using the coefficient of determination (R^2) and root-mean-square error (RMSE), computed with scikit-learn (Pedregosa et al., 2011) in Python 3.9. R^2 was calculated as $1 - SS\_res/SS\_tot$, where SS_res is the residual sum of squares between modelled and observed values, and SS_tot is the total sum of squares relative to the observed mean. RMSE was calculated as the square root of the mean squared difference between

https://doi.org/10.5194/egusphere-2026-2804
Preprint. Discussion started: 28 July 2026

modelled and observed GPP, providing a measure of absolute prediction error in the same units as the data.

Table 3. Characteristics of the sites used for the seasonal and diurnal cycle analyses.

Site name	Site ID	Latitude	Longitude	Elevation (m)	MAT (°C)	MAP (mm)	Seasonal cycle
Hyytiälä	FI-Hyy	61.85°N	24.29°E	181	3.5	711	Jan 2011–Dec 2014
Vielsalm	BE-Vie	50.31°N	6.00°E	490	8.2	916	Jan 2011–Dec 2014
Univ. of Michigan Biological Station	US-UMB	45.56°N	84.71°W	234	5.5	800	2011, 2012, 2014 (Jan–Dec)
French Guiana	GF-Guy	5.28°N	52.93°W	40	26.0	3000	2007, 2009, 2013, 2014 (Jan–Dec)
Chamau	CH-Cha	47.21°N	8.41°E	393	10.0	1100	Jan 2011–Dec 2014
Grillenburg	DE-Gri	50.95°N	13.51°E	385	8.4	877	Jan 2011–Dec 2014
Fyodorovskoye	RU-Fyo	56.46°N	32.92°E	270	3.9	730	Jan 2011–Dec 2014

2.5 Sensitivity Analysis

A sensitivity analysis was conducted at C_3 grass-dominated sites to isolate the contribution of individual PFT-specific parameters to differences in simulated GPP between PFTs. In each experiment, the land surface was prescribed as 100% C_3 grass or 100% broadleaf tree cover, removing the influence of mixed tile fractions. We examined three PFT-specific parameters: the top leaf nitrogen concentration (n_{l0}), the leaf scattering coefficient (Ω), and the light extinction coefficient. In each experiment, a single parameter was substituted from its default grass value to the corresponding broadleaf tree value, while all other parameters were held constant. Four model configurations were evaluated: (1) a control run using default C_3 grass

https://doi.org/10.5194/egusphere-2026-2804
Preprint. Discussion started: 28 July 2026

parameters; (2) grass parameters with tree n_{10}; (3) grass parameters with tree Ω; and (4) grass parameters with tree extinction coefficient.

3. Results

3.1 Evaluation of simulated gross primary production

Comparison of observed and modelled GPP at monthly and annual timescales shows that the PJULES performs better than both multi-layer configurations (Fig. 1). At the monthly scale (Fig.1a), PJULES has an R^2 of 0.62 and an RMSE of 2.24 g C m^{-2} d^{-1}, compared to R^2 values of 0.53 and RMSE of 2.54 g C m^{-2} d^{-1} for both multi-layer configurations. The regression slope (0.81) of PJULES is considerably closer to the 1:1 line than those of the multi-layer models (0.54), indicating that the latter systematically underestimate GPP across the observed range. Differences in model performance between the three configurations are more pronounced at the annual scale (Fig.1b): PJULES has an R^2 of 0.50 and an RMSE of 1.38 g C m^{-2} d^{-1}, while the both multi-layer configurations show a decline in explanatory power (JULES-GL7: R^2 = 0.20, JULES-UKESM1: R^2 = 0.17) and higher RMSE values (JULES-GL7: 1.78 g C m^{-2} d^{-1}; JULES-UKESM1: 1.81 g C m^{-2} d^{-1}). However, the JULES-UKESM1 configuration has a regression slope that is marginally closer to the 1:1 line than JULES-GL7. Overall, increasing the number of PFTs does not result in improved performance.

https://doi.org/10.5194/egusphere-2026-2804
Preprint. Discussion started: 28 July 2026

Figure 1. Correlation of observed and modelled (a) monthly and (b) yearly gross primary production (GPP, g C m^{-2} d^{-1}) across all 134 PLUMBER2 sites for the PJULES, GL7 and UKESM1 configurations.

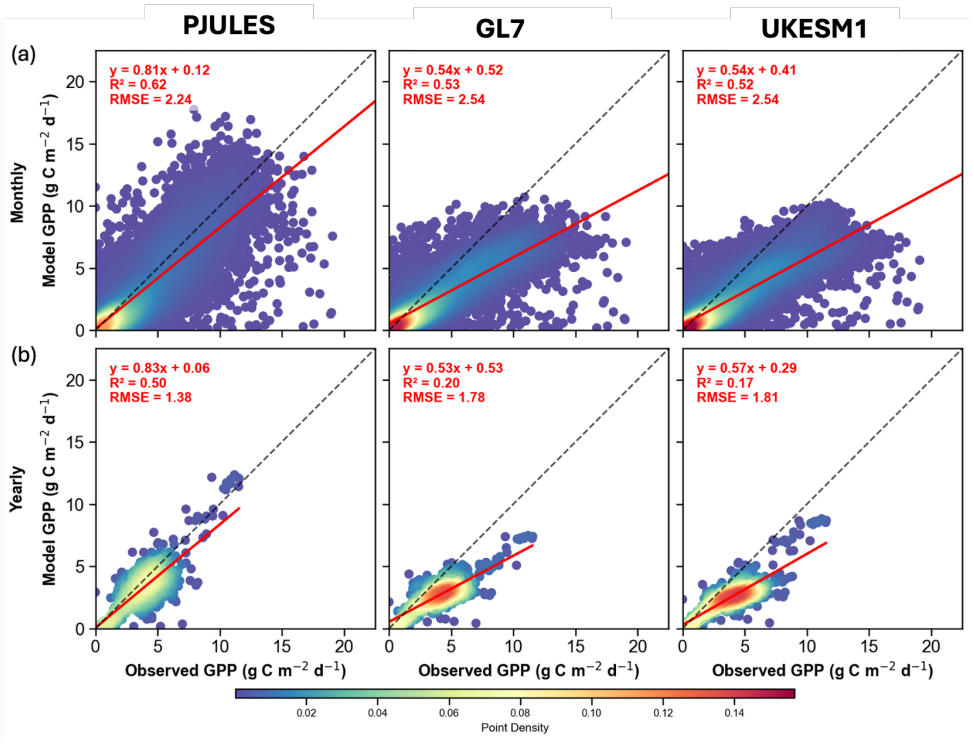

The performance of all three model configurations declines with increasing aridity (Fig. 2), such that the underestimation of GPP increases progressively. Nevertheless, PJULES outperforms both multi-layer configurations at humid sites (Fig. 2a) at the monthly scale (R^2 = 0.66, RMSE = 2.15 g C m^{-2} d^{-1}, slope = 0.89). JULES-GL7 (R^2 = 0.54, RMSE = 2.54 g C m^{-2} d^{-1}, slope = 0.57) and JULES-UKESM1 (R^2 = 0.53, RMSE = 2.56 g C m^{-2} d^{-1}, slope = 0.59) show similar performance at these sites. PJULES also performs better (R^2 = 0.46, RMSE = 1.57 g C m^{-2} d^{-1}, slope = 0.72) at semi-arid sites (Fig. 2b) than either JULES-GL7 (R^2 = 0.39, RMSE = 1.66 g C m^{-2} d^{-1}, slope = 0.51) or JULES-UKESM1 (R^2 = 0.47, RMSE = 1.56 g C m^{-2} d^{-1}, slope = 0.55). The improved performance of JULES-UKESM1 compared to JULES-GL7 for semi-arid sites at the monthly timescale is also characteristic of arid sites (Fig. 2c), where it outperforms (R^2 = 0.31, RMSE = 0.86 g C m^{-2} d^{-1}, slope = 0.32) both JULES-GL7 (R^2 = 0.19, RMSE = 0.93 g C m^{-2} d^{-1}, slope = 0.28) and PJULES (R^2 = 0.08, RMSE = 0.99 g C m^{-2} d^{-1}, slope = 0.23).

https://doi.org/10.5194/egusphere-2026-2804
Preprint. Discussion started: 28 July 2026

Comparisons at the annual scale are consistent with the pattern shown at the monthly timescale (Fig. S1): performance declines progressively with increasing aridity across all three configurations. Indeed, at both arid (Fig. S1c). and semi-arid (Fig. S1b) sites all three configurations have negative R^2 values and low explanatory power. PJULES performs reasonably well at humid sites (Fig. S1a), with an $R^2 = 0.42$, RMSE=1.42 g C m^{-2} d^{-1} and slope = 0.8, which are better than both JULES-GL7 and JULES-UKESM1with a slope around 0.5.

Figure 2. Comparison of monthly modelled and observed gross primary production (GPP) at the monthly scale across different aridity classes: (a) humid (aridity index, AI, < 2), (b) semi-arid (AI between 2 and 5) and arid (AI >5).

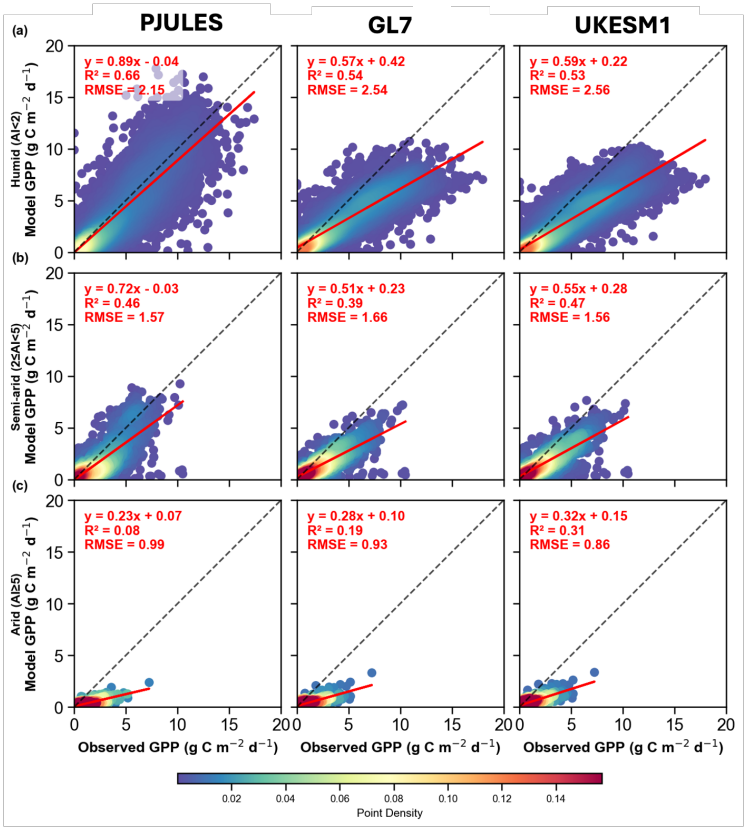

Evaluation of the seasonal cycle of GPP in the northern hemisphere (Fig. 3a) shows that PJULES has a better performance than either of the multi-layer configurations in summer (JJA), autumn (SON) and winter (DJF). It overestimates GPP in JJA by only 6% (8.17 vs 7.71 g C m^{-2} d^{-1}), compared to the JULES-GL7 and JULES-UKESM1 configurations which

https://doi.org/10.5194/egusphere-2026-2804
Preprint. Discussion started: 28 July 2026

underestimate GPP in summer by 36% and 38% respectively. PJULES slightly overestimates GPP in autumn by 2% (3.04 vs 2.98 g C m^{-2} d^{-1}), while JULES-GL7 and JULES-UKESM1 underestimate GPP in SON by 34% and 37% respectively. All three configurations underestimate GPP in winter, but the underestimation in PJULES is only 14% (0.95 vs 1.11 g C m^{-2} d^{-1}) compared to 43% in JULES-GL7 and 55% in JULES-UKESM1. While the two multi-layer configurations also underestimate GPP in spring, PJULES shows a large overestimation of GPP by 33% (5.08 vs 3.81 g C m^{-2} d^{-1}). The tendency for the P-model to overestimate GPP during the early part of the year has also been observed in standalone simulations (e.g. Zhou et al., 2025). The observed seasonal cycle of GPP is more muted in the Southern Hemisphere sites (3.33–6.36 g C m^{-2} d^{-1}) than in the Northern Hemisphere sites (1.11–7.71 g C m^{-2} d^{-1}) (Fig.3b; Table S4). PJULES is close to the 1:1 line in all seasons, whereas both multi-layer configurations underestimate GPP across all seasons. Consistent with seasonal biases in the Northern Hemisphere, PJULES shows the smallest overestimation in MAM (5.17 vs 4.95 g C m^{-2} d^{-1}, 4%) and the largest in SON (5.60 vs 4.97 g C m^{-2} d^{-1}, 13%).

Figure 3. Comparison of seasonal mean gross primary production (GPP) for (a) sites in the Northern Hemisphere and (b) sites in the Southern Hemisphere. Colours represent different model configurations: PJULES (brown), JULES-GL7 (tan), and JULES-UKESM1 (blue). Symbols represent the four seasons: March-April-May, MAM (diamonds), June-July-August, JJA (circles), September-October-November, SON (triangles), and December-January-February, DJF (squares). The dashed black line indicates the 1:1 relationship between modelled and observed GPP.

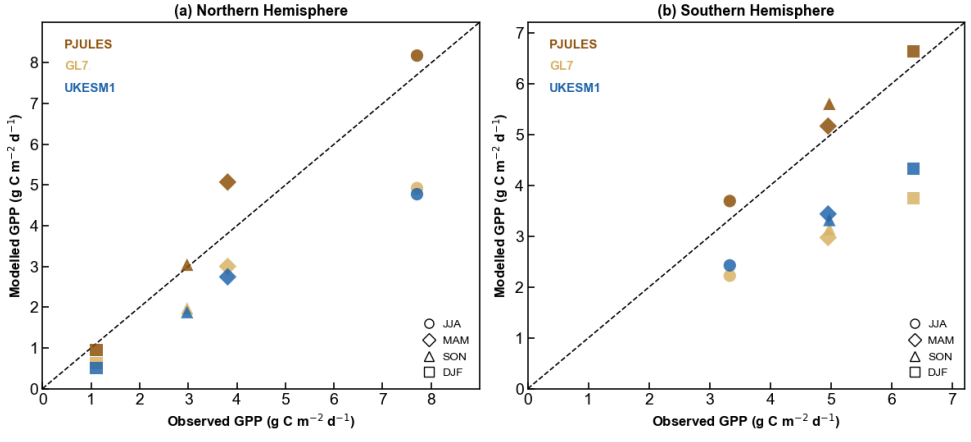

https://doi.org/10.5194/egusphere-2026-2804
Preprint. Discussion started: 28 July 2026

Comparison of the seasonal cycle at individual flux tower sites (Fig. 4) provides further confirmation that PJULES performs better than the JULES-GL7 and JULES-UKESM1 configurations, both of which consistently underestimate the observed GPP. The tendency for PJULES to green-up too early and hence overestimate GPP during spring can be clearly observed at the four temperate forest sites (US-UMB, BE-Vie, RU-Fyo and FI-Hyy). PJULES simulates GPP that closely matches the observations during the first part of the year (up to day 200) at the tropical forest site (GF-Guy), whereas the JULES-GL7 and JULES-UKESM1 configurations considerably underestimate GPP. All three configurations show an increase in GPP after day 200, which in the case of PJULES results in a considerable overestimation of GPP compared to the observations, which show a general reduction over the second part of the year. The JULES-GL7 and JULES-UKESM1 configurations underestimate GPP at other tropical sites (Fig. S2). PJULES reduces this persistent low bias, although in some cases this results in an overestimation of GPP during some part of the year (Fig. S2). PJULES performs better overall than the two multi-layer configurations at the two grassland sites (CH-Cha, DE-Gri). However, all three configurations fail to capture the mid-summer drop in observed GPP at DE-Gri.

Figure 4. Mean seasonal cycle of gross primary production (GPP) at selected FLUXNET sites, representing tropical forest (GF-Guy) boreal forest (FI-Hyy, RU-Fyo), mixed forest (BE-Vie), temperate forest (US-UMB) and grassland (CH-Cha, DE-Gri).

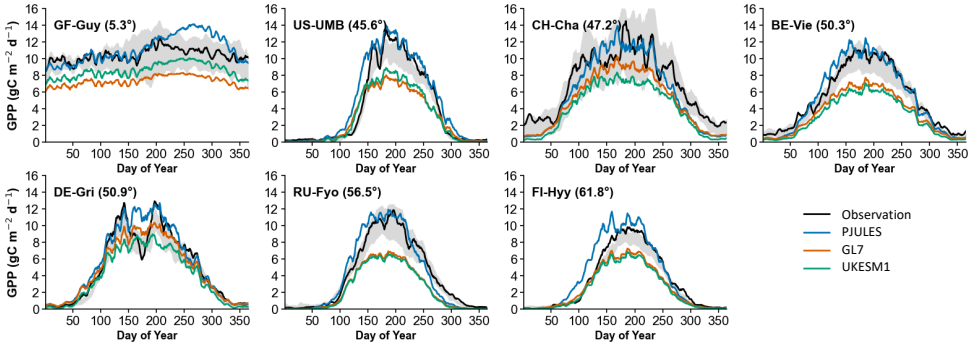

PJULES tracks the observed diurnal cycle reasonably well at the boreal, mixed and temperate forest sites (Fig. 5). In contrast, the two multi-layer configurations tend to underestimate GPP during most of the day, particularly at US-UMB and RU-Fyo. PJULES has an $R^2 = 0.89$ and RMSE = 3.6 µmol m^{-2} s^{-1} at US-UMB, compared to JULES-GL7 ($R^2 = 0.50$, RMSE = 7.6 µmol m^{-2} s^{-1}) and JULES-UKESM1 ($R^2 = 0.67$, RMSE = 6.2 µmol m^{-2} s^{-1}). Similarly, PJULES

https://doi.org/10.5194/egusphere-2026-2804
Preprint. Discussion started: 28 July 2026

has an $R^2 = 0.80$ and RMSE = 4.3 μmol m^{-2} s^{-1} at RU-Fyo, considerably outperforming JULES-GL7 ($R^2 = 0.40$, RMSE = 7.3 μmol m^{-2} s^{-1}) and JULES-UKESM1 ($R^2 = 0.38$, RMSE = 7.4 μmol m^{-2} s^{-1}). PJULES also captures the observed diurnal GPP dynamics at BE-Vie more accurately (BE-Vie: $R^2 = 0.91$, RMSE = 2.5 μmol m^{-2} s^{-}) than either of the multi-layer configurations (JULES-GL7: $R^2 = 0.77$, JULES-UKESM1: $R^2 = 0.70$). The degradation in performance between JULES-GL7 and JULES-UKESM1 again confirms that additional complexity in terms of number of PFTs does not result in improved performance. Differences between the three configurations are smallest at the boreal forest site (FI-Hyy), although the P-model still shows better performance ($R^2 = 0.91$, RMSE = 2.0 μmol m^{-2} s^{-1}) than either JULES-GL7 ($R^2 = 0.81$, RMSE = 2.8 μmol m^{-2} s^{-1}) or UKESM1 ($R^2 = 0.78$, RMSE = 3.1 μmol m^{-2} s^{-1}). However, UKESM1 has the best performance at the tropical forest site, GF-Guy ($R^2 = 0.91$, RMSE = 3.6 μmol m^{-2} s^{-1}), outperforming both the PJULES ($R^2 = 0.79$, RMSE = 5.7 μmol m^{-2} s^{-1}) and JULES-GL7 ($R^2 = 0.79$, RMSE = 5.7 μmol m^{-2} s^{-1}) configurations. PJULES performs well at one of the grassland sites (CH-Cha) with an $R^2 = 0.86$, RMSE = 5.0 μmol m^{-2} s^{-1}, whereas the R^2 for JULES-GL7 is only 0.72 and that for JULES-UKESM1 only 0.62. All three configurations perform poorly at the DE-Gri grassland site, with R^2 ranging from −0.95 (PJULES) to 0.16 (JULES-UKESM1).

https://doi.org/10.5194/egusphere-2026-2804
Preprint. Discussion started: 28 July 2026

Figure 5. Comparison of simulated gross primary production (GPP) by the PJULES, JULES-GL7 and JULES-UKESM1 configurations for a single week in August 2014 at selected FLUXNET sites. The sites are organised by latitude from the tropics (top) to the boreal zone (bottom).

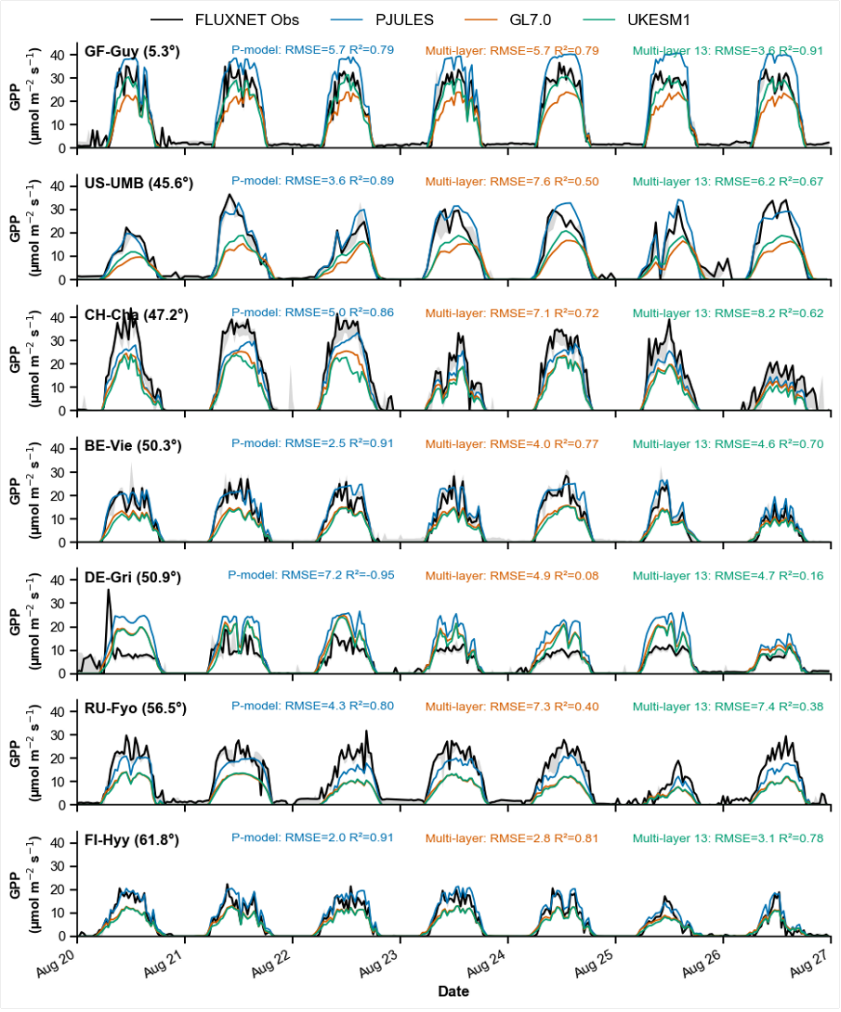

Site mean GPP is underestimated by both PJULES and JULES-GL7 when considering the four C_3 PFTs in the GL7 configuration (Table 3). However, PJULES generally demonstrates closer agreement with observations and lower error metrics. At the needleleaf tree (NT) sites, where the observed mean GPP is 4.11 g C m^{-2} d^{-1}, the PJULES value is much better (3.53 g C m^{-2} d^{-1}) than JULES-GL7 (2.23 g C m^{-2} d^{-1}) and the PJULES RMSE (1.38 g C m^{-2} d^{-1}) is substantially lower than JULES-GL7 (2.18 g C m^{-2} d^{-1}), indicating significantly better

https://doi.org/10.5194/egusphere-2026-2804
Preprint. Discussion started: 28 July 2026

performance. At broadleaf tree (BT) sites, where the observed mean GPP is 4.78 g C m^{-2} d^{-1}, PJULES simulates 4.13 g C m^{-2} d^{-1} compared to 3.07 g C m^{-2} d^{-1} for JULES-GL7. The RMSE values for the two configurations are similar (1.90 and 2.09 g C m^{-2} d^{-1}, respectively), but PJULES has a smaller systematic bias. At the shrub sites, PJULES (3.43 g C m^{-2} d^{-1}) is closer to observations (3.86 g C m^{-2} d^{-1}) than JULES-GL7 (2.61 g C m^{-2} d^{-1}), and the RMSE (1.02 g C m^{-2} d^{-1}) is also lower than JULES-GL7 (1.25 g C m^{-2} d^{-1}). The underestimation of GPP at C_3 grass sites (3.07 g C m^{-2} d^{-1}) is smaller in JULES-GL7 (2.32 g C m^{-2} d^{-1}) than in PJULES (2.29 g C m^{-2} d^{-1}). JULES-GL7 also has a smaller RMSE compared to PJULES (1.16 vs 1.36 g C m^{-2} d^{-1}), showing somewhat better representation of this PFT. The systematic differences between PJULES and JULESGL7, with PJULES showing better performance for sites dominated by woody plants and JULES-GL7 for C_3 grassland reflects fundamental differences in parameterization between these two vegetation types.

PJULES performs better than JULES-UKESM1 in 6 out of 7 C_3 PFTs represented in the UKESM1 configuration in terms of both mean GPP and RMSE (Table S2). The exception is tropical broadleaf evergreen tree, where JULES-UKESM1 underestimates (7.05 g C m^{-2} d^{-1}) but is closer to the observed site mean value (7.89 g C m^{-2} d^{-1}) than PJULES (8.85 g C m^{-2} d^{-1}). However, PJULES has a slightly better RMSE than JULES-UKESM1 (1.50 vs 1.60 g C m^{-2} d^{-1}). JULES-GL7 had better performance for C_3 grass than PJULES (Table 3) but in the UKESM1 configuration where C_3 grass sites are separated into C_3 grass and C_3 crop, this advantage disappears: both models show similar performance for C_3 grass with the same RMSE values (1.36 g C m^{-2} d^{-1}) although PJULES had a marginally smaller mean bias.

https://doi.org/10.5194/egusphere-2026-2804
Preprint. Discussion started: 28 July 2026

Table 3. Summary of site mean gross primary production (GPP) and variability across all sites for the four C_3 plant functional types (PFTs) considered in the JULES-GL7 configuration: broadleaf tree (BT), needleleaf tree (NT), C_3 grass and shrub.

PFT	Mean GPP			RMSE	
	Obs	PJULES	GL7	PJULES	GL7
BT	4.78	4.13	3.07	1.90	2.09
NT	4.11	3.53	2.23	1.38	2.18
C_3 grass	3.07	2.29	2.32	1.36	1.16
shrub	3.86	3.43	2.61	1.02	1.25

Sensitivity analyses (Fig. 6) show that the differences in simulated GPP between grass and tree largely reflect the differences in parameter values used for n_{10} and Ω. Replacing the light extinction coefficient (grass value with that of trees) had no significant effect on simulated GPP ($p = 0.93$), confirming that differences in canopy light attenuation between PFTs are negligible at C_3 grassland sites. Substituting the Ω parameter, which affects leaf-level CO_2 assimilation, resulted in a small but statistically significant reduction in mean GPP (-0.05 g C m^{-2} d^{-1}, $p < 0.001$). The largest effect on GPP was produced by substituting the top-leaf nitrogen concentration (n_{10}) with the tree equivalent, which resulted in a significant reduction in simulated GPP from a mean value of 3.14 g C m^{-2} d^{-1} in the control to 2.58 g C m^{-2} d^{-1} (mean difference = -0.56 g C m^{-2} d^{-1}, $p < 0.001$), closely approaching the Reference Pure Tree mean of 2.49 g C m^{-2} d^{-1} (Fig. 8). This confirms that n_{10}, through its control on V_{cmax25}, is the dominant parameter driving the GPP difference between grass and tree simulations in the GL7 scheme.

https://doi.org/10.5194/egusphere-2026-2804
Preprint. Discussion started: 28 July 2026

Figure 6. Sensitivity test of GPP to PFT parameterizations. The control represents the original pure grass setup, while the reference shows the potential productivity of a pure tree setup.

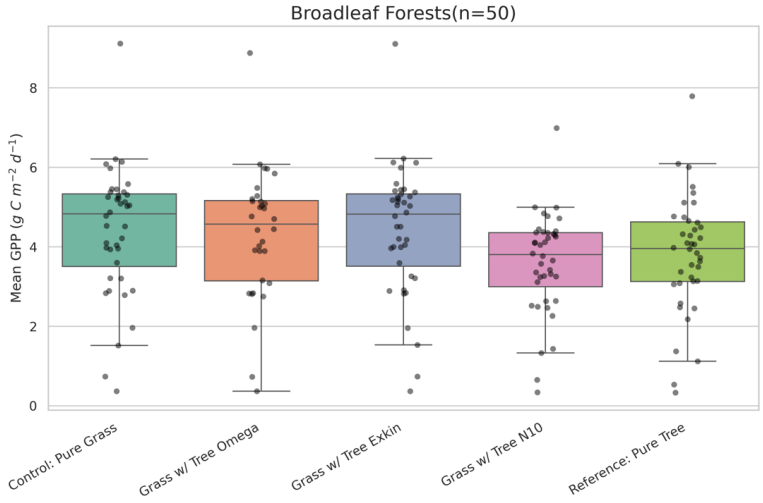

3.2 Evaluation of latent heat flux

Comparison of observed and modelled LE across monthly and yearly timescales for all three configurations (Fig. 7) shows that PJULES has similar explanatory power to JULES-UKESM1 but produces more realistic fluxes than JULES-GL7. At the monthly scale (Fig. 7a), PJULES has an R^2 of 0.68 and RMSE of 18.96 W m^{-2}, close to the values for JULES-UKESM1 (R^2 = 0.69, RMSE = 18.18 W m^{-2}) and better than GL7 (R^2 = 0.64, RMSE = 19.15 W m^{-2}). The regression slopes indicate a systematic tendency to underestimate LE at higher observed values, although PJULES (0.82) is marginally closer to the 1:1 line than either UKESM1 (0.78) or the JULES-GL7 (0.76) configuration. Differences between the three configurations at the yearly scale are small but consistent. PJULES and JULES-UKESM1 show similar explanatory power (R^2 = 0.64 and 0.65, respectively), and both are better than JULES-GL7 (R^2 = 0.52) (Fig.7b). The same pattern is seen in the RMSE values: JULES-UKESM1 has the lowest RMSE (11.97 W m^{-2}), PJULES is intermediate (12.21 W m^{-2}) and JULES-GL7 has the highest RMSE (13.26 W m^{-2}).

https://doi.org/10.5194/egusphere-2026-2804
Preprint. Discussion started: 28 July 2026

Figure 7. Correlation of observed and modelled (a) monthly and (b) yearly latent heat (LE) values of all studied sites, for the PJULES, GL7 and UKESM1 configurations.

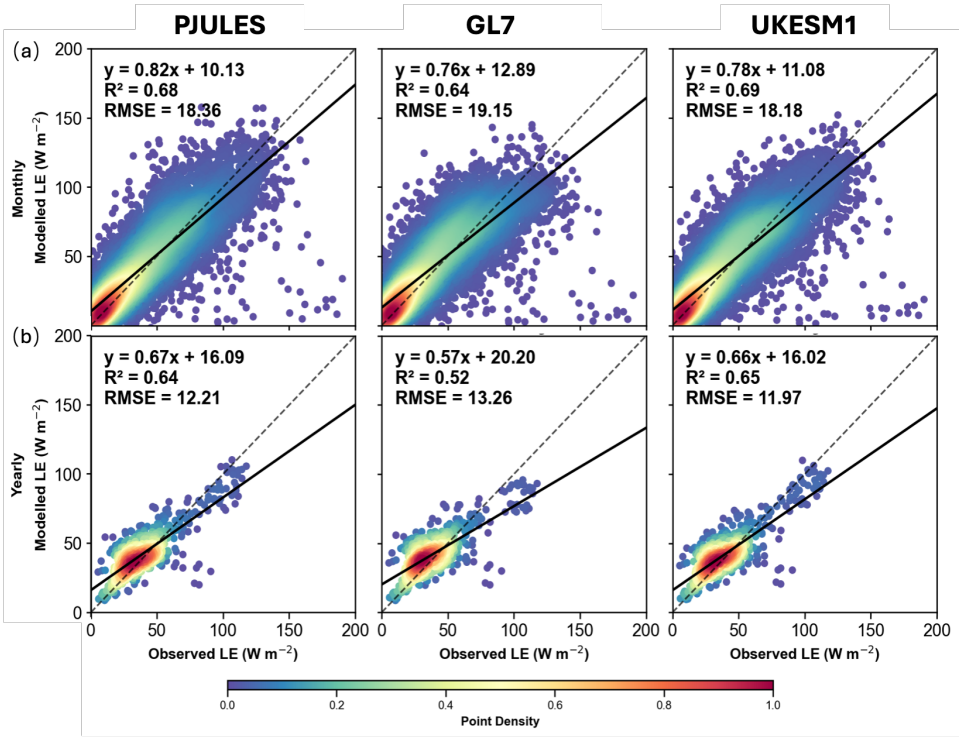

As is the case with simulated GPP, PJULES performance for LE degrades with increasing aridity. PJULES has a slope of 0.88 at humid sites (AI < 2) and is closest to the 1:1 line at the monthly time scale (Fig. 8a), while JULES-GL7 (slope=0.76) and JULES-UKESM1 (slope=0.81) underestimate LE to a greater extent, consistent with their more pronounced underestimation of GPP at these sites (Fig. 2a). At semi-arid and arid sites, however, the multi-layer configurations have slopes closer to one despite their continued underestimation of GPP (Fig. 2b, 2c), while the PJULES slopes increase to 1.02 at semi-arid and 1.14 at arid sites, indicating a tendency towards LE overestimation under water-limited conditions (Fig. 8b-c). This suggests that the multi-layer models exhibit a degree of decoupling between carbon assimilation and water fluxes under water limitation. PJULES shows the opposite pattern at arid sites, with GPP underestimated and LE overestimated, which is unlikely to result from stomatal limitation alone and may instead reflect an overestimation of bare soil evaporation.

https://doi.org/10.5194/egusphere-2026-2804
Preprint. Discussion started: 28 July 2026

Figure 8. Comparison of monthly modelled and observed latent heat flux (LE) at the monthly scale across different aridity classes: (a) humid (aridity index, AI, < 2), (b) semi-arid (AI between 2 and 5) and arid (AI ≥ 5).

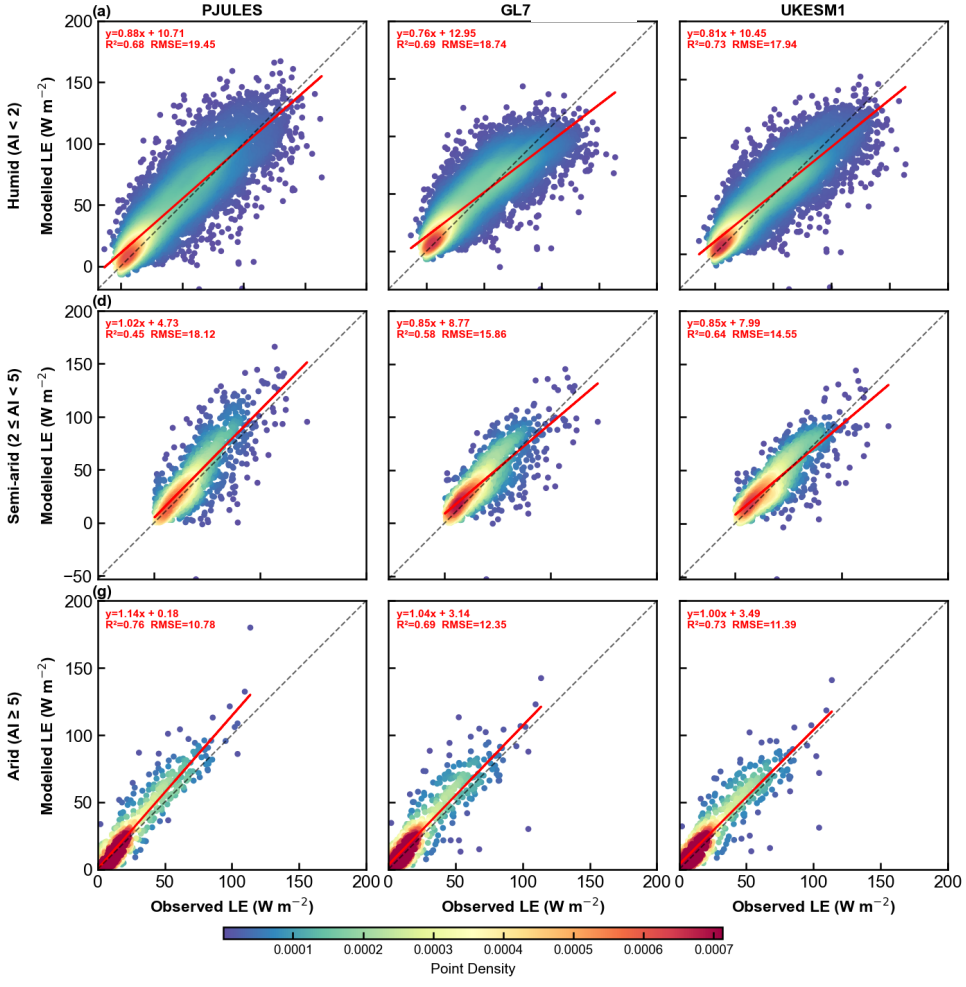

Seasonal mean LE is relatively well reproduced in sites in both hemispheres in all of the configurations, with R^2 values of 0.61–0.66 and RMSE of 18.30-19.51 W m^{-2} in the Northern Hemisphere sites and 0.58–0.66 and 21.83–23.88 W m^{-2} in the Southern Hemisphere sites (Tables S5–S6, Fig. 9). All three configurations have LE values above the observed mean in all seasons in the Northern Hemisphere. PJULES has a large positive bias in JJA (76.48 W m^{-2}), but JULES-GL7 and JULES-UKESM1 are closer to observations (68.32 W m^{-2}) with values of 69.53 and 68.71 W m^{-2} respectively. The overestimation of both GPP and LE in JJA in PJULES suggests a coupled response in which the optimality-based scheme drives both

https://doi.org/10.5194/egusphere-2026-2804
Preprint. Discussion started: 28 July 2026

carbon and water fluxes in the same direction. This coupling is expected from the underlying equations linking photosynthesis and stomatal conductance; however, the response is non-linear, such that the substantial improvement in GPP under PJULES does not result in an overestimation of ET. This is not seen in the multi-layer configurations, where the LE is close to observed values but observed GPP (7.20 g C m^{-2} d^{-1}) is considerably underestimated. This is likely due to the soil moisture stress factor (β) causing an overly strong constraint on assimilation as well as the lack of acclimation (GL7: 4.64 g C m^{-2} d^{-1}; UKESM1 4.50 g C m^{-2} d^{-1}). All three configurations underestimate LE in the Southern Hemisphere sites, with the largest bias again in summer (DJF). However, the PJULES estimate (91.18 W m^{-2}) is closer to the observed mean value of 91.30 W m^{-2} than either JULES-GL7 (77.04 W m^{-2}) or JULES-UKESM1 (86.33 W m^{-2}).

Figure 9. Comparison of seasonal mean latent heat (LE) for (a) sites in the Northern Hemisphere and (b) sites in the Southern Hemisphere. Colours represent different model configurations: PJULES (brown), GL7 (tan), and UKESM1 (blue). Symbols denote the four seasons: JJA (circles), MAM (diamonds), SON (triangles), and DJF (squares). The dashed black line indicates the 1:1 relationship between modelled and observed LE.

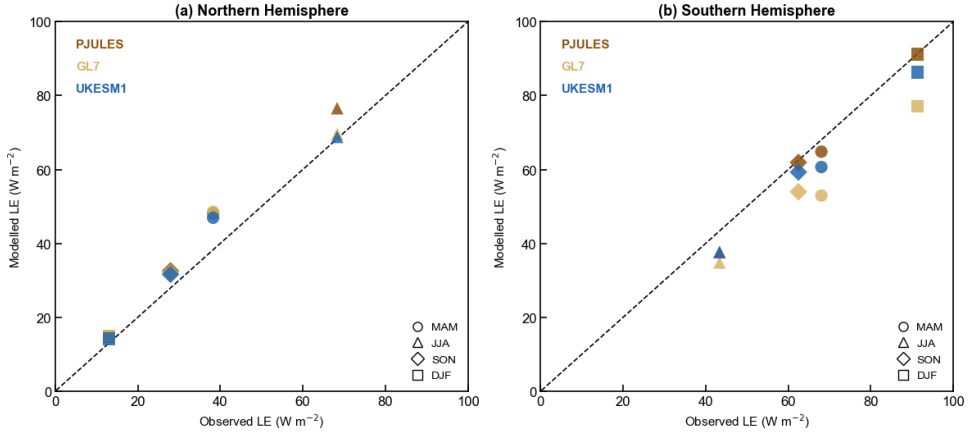

The seasonal cycle of LE is well captured across most sites, with smaller differences between the three configurations than for GPP (Fig. 10). The match to the observed seasonal cycle and timing is best for the extratropical forest sites (RU-Fyo, BE-Vie) and the CH-Cha grassland site. PJULES produces a close match to observations at the tropical forest site (GF-Guy) for the first part of the year but shows a slight overestimation in the second half of the year, when

https://doi.org/10.5194/egusphere-2026-2804
Preprint. Discussion started: 28 July 2026

GPP was also overestimated. In contrast, the multi-layer configurations underestimate LE throughout the year. All three configurations overestimate LE at the US-UMB and FI-Hyy sites during early spring (approximately day 50–150). This corresponds to the period when PJULES overestimates GPP, but the multi-layer configurations do not show an overestimation in GPP (Fig.4) again pointing to the decoupling between carbon assimilation and water fluxes. The mid-summer drop in observed LE at the DE-Gri grassland site is not captured by any of the three configurations.

Figure 10. Mean seasonal cycle of latent heat (LE) at each of the selected FLUXNET sites

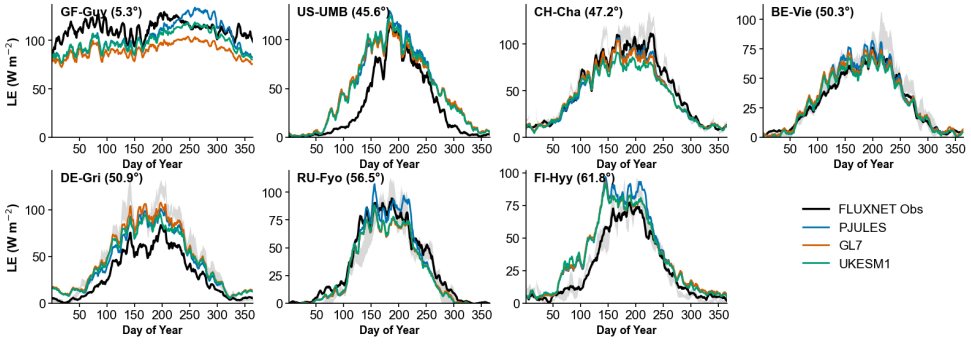

The diurnal cycle of LE is generally well reproduced across the seven sites, with all three models capturing the midday peak in surface evapotranspiration (Fig.11). At most temperate and boreal sites (BE-Vie, RU-Fyo, FI-Hyy, CH-Cha), differences among models are small. However, PJULES overestimates peak daytime LE at US-UMB, while the multi-layer configurations track the observed midday values more closely (GL7: R^2=0.85; UKESM1: R^2=0.82; PJULES: R^2=0.69). PJULES produces a good agreement with observations at GF-Guy (R^2=0.88, RMSE=60.1 W m^{-2}), better than both JULES-UKESM1 (R^2=0.84, RMSE=70.6 W m^{-2}), and JULES-GL7 (R^2=0.77, RMSE=83.2 W m^{-2}) estimates of peak LE. PJULES also achieves the best fit to observed LE at DE-Gri (R^2=0.75, RMSE=30.1 W m^{-2}), although the simulation of the diurnal cycle at this site was as poor as the other two configurations.

https://doi.org/10.5194/egusphere-2026-2804
Preprint. Discussion started: 28 July 2026

Figure 11. Comparison of observed and simulated latent heat (LE) by PJULES the GL7 and UKESM1 model for a single week in August 2014 at each of the selected FLUXNET sites. The sites are organised by latitude from the tropics (top) to the boreal zone (bottom).

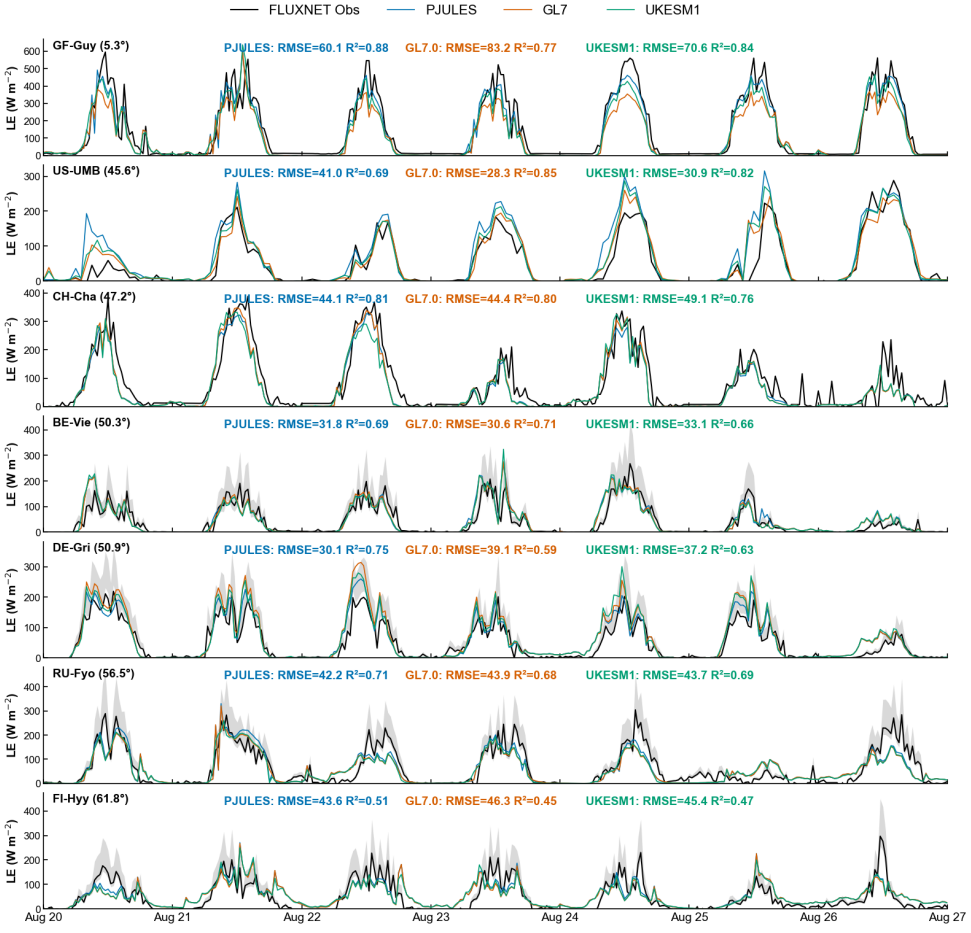

4. Discussion

PJULES performs better overall than either of the JULES multi-layer configurations. The improvements in simulated GPP produced by PJULES are not accompanied by a degradation in LE, suggesting that the optimality-based approach produces a more physically consistent representation of surface carbon and water fluxes. The marginal performance gain from expanding from 5 to 13 PFTs in the JULES standard configurations suggests that additional structural complexity does not translate into improved predictive skill, a challenge widely recognised in land surface modelling (Blyth et al., 2021; Fisher and Koven, 2020; Raoult et al.,

https://doi.org/10.5194/egusphere-2026-2804
Preprint. Discussion started: 28 July 2026

2025). The consistently stronger performance of PJULES across most vegetation types and time scales indicates that the optimality-based approach offers a promising and parsimonious alternative to parameter-intensive multi-layer configurations. Moreover, because the EEO-based approach does not rely on static parameters derived from observations, it is naturally better suited for climate change applications where environmental conditions may move beyond the range of current observations.

Model performance declined with increasing aridity across all three configurations. PJULES achieved the best performance at humid sites, while the two multi-layer models greatly underestimated GPP. The performance of PJULES was also better at semi-arid sites, although the differences between the three configurations were smaller. However, JULES-UKESM1 performed better than PJULES at arid sites. The overall degradation of model performance under high aridity reflects the use of the β function in the JULES framework. In this framework, soil moisture stress is applied through a universal piecewise linear β function of volumetric water content (Clark et al., 2011) . Vegetation is assumed to not be stressed when soil moisture is above field capacity (−0.033 MPa), but GPP declines linearly towards zero at the wilting point below this threshold (Best et al., 2011; Cox et al., 1999). This function is applied across all ecosystems regardless of their climatic context (Harper et al., 2021). This is inconsistent with observed ecosystem behaviour: plants adapted to more arid climates use water more conservatively when soil moisture is high, but maintain GPP down to lower critical soil moisture thresholds than humid ecosystems (Bassiouni et al., 2020; Fu et al., 2024; Stocker et al., 2018). Furthermore, even in relatively humid European ecosystems, the observed soil matric potential threshold at which plant water stress begins is approximately 0.71 MPa (Fu et al., 2022), considerably more negative than the threshold used in JULES. Since PJULES uses the β parameterization from the JULES framework, the optimality-based stomatal scheme operates on a soil moisture signal that does not reflect the adaptive water-use strategies of water-limited vegetation, limiting its ability to simulate the progressive GPP decline that characterises arid ecosystems.

Mengoli et al. (2025) proposed an alternative way to incorporate soil moisture stress in an EEO context. Based on an analysis of eddy-covariance flux data from 67 sites spanning the full aridity gradient, they showed that the response of GPP to soil moisture stress varies systematically with climatic aridity rather than vegetation type. Both the maximum light-use efficiency under well-watered conditions and the critical soil moisture threshold below which

https://doi.org/10.5194/egusphere-2026-2804
Preprint. Discussion started: 28 July 2026

GPP declines decrease with increasing aridity. In humid ecosystems, the critical threshold (ψ) of relative soil moisture has a median of approximately 0.6, meaning GPP begins to decline even when soils are still moderately moist. This threshold decreased to around 0.3 at semi-arid sites and below 0.1 at arid sites. Applying these aridity-dependent functions to the sub-daily P model reduced RMSE by an average of 69.3% at arid sites and 47.3% at semi-arid sites relative to simulations with no soil moisture correction and also showed improvement at all arid sites and the majority of semi-arid and humid sites compared to the moisture stress function developed for the standard P-model by Stocker et al. (2020). This approach offers a promising way of improving the soil moisture stress function in PJULES.

PJULES consistently overestimated GPP during spring (MAM) in the Northern Hemisphere, with simulated values exceeding observations by 33% on average. This early-season high bias was also evident at the site level, particularly at the temperate deciduous forest (US-UMB), boreal needleleaf (FI-Hyy) and mixed forest (RU-Fyo), where PJULES predicted an early onset of the growing season relative to observations. This spring overestimation reflects a well-documented phenomenon, previously identified across numerous temperate and boreal sites by Stocker et al. (2020) and in global simulations (Zhou et al., 2025). One possible explanation is that the resumption of photosynthetic capacity after winter inhibition requires sustained temperatures above a critical threshold and shows a lag relative to instantaneous air temperatures (Luo et al., 2023; Mäkelä et al., 2004, 2008; Tanja et al., 2003). This delayed recovery is primarily expressed through a reduction in φ_0: under low winter temperatures and high irradiance, vegetation accumulates photoprotective pigments that suppress φ_0 through sustained non-photochemical quenching (Ensminger et al., 2004; Verhoeven, 2014). Although PJULES accounts for the instantaneous temperature dependence of φ_0 following Bernacchi et al. (2003), it does not represent the lagged recovery of φ_0 following cold acclimation. As spring temperatures rise, PJULES therefore immediately predicts higher GPP based on favourable atmospheric temperature, while actual photosynthetic capacity recovers more slowly, a mismatch that likely contributes to the observed MAM overestimation. Luo et al. (2023) addressed this by introducing a multiplicative cold-acclimation temperature modifier that scales P model GPP based on a dynamically delayed minimum air temperature. The results show a reduction in early spring GPP overestimation by 22% across temperate and boreal forest sites. This approach could provide a way to further improve the performance of PJULES.

https://doi.org/10.5194/egusphere-2026-2804
Preprint. Discussion started: 28 July 2026

PJULES performance varied across tropical sites with RMSE ranging from 0.68 to 3.71 g C m^{-2} d^{-1}. All three configurations of JULES show similar seasonal trends that diverge from observations at tropical rainforest sites, suggesting a common structural limitation rather than model-specific issues. PJULES systematically underestimated GPP at BR-Sa3, but overestimated GPP and GF-Guy and AU-Cow, where the P-model substantially overestimates GPP. This may reflect the quality of the LAI product. The PLUMBER2 data for GF-Guy and AU-Cow used Copernicus LAI, while BR-Sa3 relies on MODIS LAI. Previous studies have shown that Copernicus systematically overestimates LAI by approximately 2 units in tropical forest regions compared to MODIS, while the two products show better agreement in sparse vegetation and semi-arid regions (Jiang et al., 2020). This systematic difference propagates directly into fAPAR and hence GPP. Thus, the overestimation of GPP by PJULES at AU-Cow probably reflects inflated LAI inputs, while the underestimation at BR-Sa3 reflects the well-documented tendency of MODIS to underestimate LAI in tropical forests where clouds cause data gaps and degradation in the satellite retrievals (Morton et al., 2014; Saleska et al., 2003).

There are systematic differences between PJULES and JULES-GL7 across PFTs. PJULES not only achieved lower RMSE but also produced higher simulated mean GPP for broadleaf trees, needleleaf trees and shrubs, but JULES-GL7 produced higher simulated mean GPP and lower RMSE in C_3 grasslands than PJULES. Since PJULES does not differentiate between tree and grass PFTs, these different patterns presumably result from differences in PFT-specific parameterisation in the multi-layer scheme. Substituting tree for grass top leaf nitrogen content (n_{l0}) resulted in a reduction in simulated C_3 grassland GPP from 3.14 to 2.58 g C m^{-2} d^{-1}, showing that n_{l0}, through its control on V_{cmax25}, is the dominant parameter driving GPP differences between grass and tree PFTs in JULES-GL7. This suggests that a better representation of nitrogen-carbon coupling, based on a firmer theoretical basis of the linkages between nitrogen uptake, photosynthesis and biomass production (Stocker et al., 2025), should be incorporated in the multi-layer configurations to improve performance.

Beyond the finding that improvements in GPP under PJULES are not accompanied by any degradation in LE performance, the results show that LE can remain close to observations even where GPP is substantially underestimated in JULES-GL7 and JULES-UKESM. This systematic divergence between GPP and LE performance points to a structural feature of the JULES evapotranspiration scheme, whereby non-stomatal evaporative pathways buffer LE even as stomatal conductance and carbon assimilation are suppressed. One such compensation

https://doi.org/10.5194/egusphere-2026-2804
Preprint. Discussion started: 28 July 2026

pathway arises because stomatal closure raises surface temperature, which increases the saturated vapour pressure at the surface, thereby generating greater soil evaporation. The underestimation of GPP in the multi-layer configurations at humid sites is mirrored by a corresponding underestimation of LE, suggesting that the two fluxes remain broadly coupled. The optimality-based stomatal scheme in PJULES produces a more physically consistent representation of both carbon and water fluxes under well-watered conditions. However, the multi-layer configurations substantially underestimate GPP at semi-arid sites yet have LE slopes close to one, while PJULES reproduces GPP more accurately but has LE slopes exceeding 1.0. All three configurations simulate GPP slopes of approximately 0.2 at arid sites but all produce LE slopes at or above 1.0, indicating that LE is largely maintained independently of carbon assimilation even under severe water limitation. This reduced coupling between plant transpiration and total ET suggests that the representation of evapotranspiration and its component fluxes in JULES may be a source of bias. While global observations indicate transpiration is about 62% of total terrestrial evaporation (Miralles et al., 2025), transpiration represents only 42% of total evapotranspiration in the standard JULES configuration, and the rest is from evaporation from the soil or intercepted water (Van den Hoof et al., 2013). The β soil moisture stress function is applied directly to leaf-level photosynthesis in all the JULES configurations, which suppresses both GPP and, through the coupled A-g_s scheme, stomatal conductance and transpiration. However, soil evaporation is driven primarily by the availability of energy at the soil surface and the moisture content of the topsoil layer, both of which are independent of stomatal function. As a result, total LE can be buffered by these non-stomatal pathways even as GPP and transpiration are suppressed by soil moisture stress, although the magnitude of this compensation is unclear.

LAI is likely to play an important role in modulating the partitioning of LE more generally across all three configurations. In arid and semi-arid ecosystems, a greater fraction of incoming radiation reaches the soil surface because LAI is low and canopy shading reduced. This would sustain or even increase soil evaporation even as transpiration declines under water stress (Harper et al., 2021). Furthermore, reduced transpiration increases soil water availability through greater infiltration, which can in turn sustain higher rates of soil evaporation. In contrast, intercepted water evaporation decreases with lower LAI as the canopy water storage capacity is reduced, meaning that the two non-stomatal components of LE respond in opposing directions to changes in vegetation cover (Van den Hoof et al., 2013). The net effect on total

https://doi.org/10.5194/egusphere-2026-2804
Preprint. Discussion started: 28 July 2026

LE therefore depends on the relative magnitude of these two processes and will vary not only with vegetation cover but also with soil texture and atmospheric evaporative demand.

The current evaluation is based on historical FLUXNET observations. Future climate projections indicate substantially higher temperatures under high-emission scenarios, which would provide a more stringent test of the robustness of PJULES under warmer and high CO_2 conditions. A further limitation of the current study is the absence of C_4 vegetation in the PJULES configuration. C_4 plants account for between 19-23% of global GPP (Luo et al., 2024; Still et al., 2003) and dominate tropical savannahs and grasslands where warming is projected to be most pronounced. The implementation of a C_4 photosynthesis pathway in PJULES would therefore be an important step towards a more complete global assessment.

5. Conclusion

This study evaluated PJULES compared to JULES-GL7, and JULES-UKESM1 across FLUXNET sites within the PLUMBER2 framework. PJULES demonstrated consistently better performance with improvements in GPP simulation unaccompanied by degradation in LE, suggesting a more physically consistent representation of surface carbon and water fluxes. The marginal performance gain from expanding from 5 to 13 PFTs for the two multilayer JULES configurations suggests that increased model complexity does not necessarily translate into improved predictive skill. Extension of the evaluation to future climate scenarios and implementation of C_4 photosynthesis in PJULES represent important priorities for strengthening the global applicability of these configurations.

Code and data availability

The JULES land surface model is developed and maintained in the Met Office Science Repository Service (MOSRS; https://code.metoffice.gov.uk). The model code is freely available to any researcher who registers for a MOSRS account. JULES vn7.0 was used for the GL7 configuration and JULES vn7.8 for the UKESM1 configuration. Model documentation is available at https://jules-lsm.github.io/vn7.0/ and https://jules-lsm.github.io/vn7.8/ (last access: 11 May 2026). The P-model implementation described in this paper is held in the JULES branch main/branches/dev/wenyaogan/r24333_pmodel at revision @25369. The site-level simulations were performed with the Rose suites u-dl036 (revision @241004, for vn7.0) and u-do085 (revision @311374, for vn7.8), available from the MOSRS roses-u repository (https://code.metoffice.gov.uk/trac/roses-u). Access to the

https://doi.org/10.5194/egusphere-2026-2804
Preprint. Discussion started: 28 July 2026

branch and the suites requires a MOSRS account, for which any researcher may register free of charge. The primary dataset underlying this study the PJULES model output together with the analysis code and scripts required to reproduce all results and figures presented in this paper is openly archived at https://doi.org/10.5281/zenodo.20344326 (Gan, 2026). The PLUMBER2 forcing and evaluation data used to drive and evaluate the simulations are available from the NCI National Research Data Collection at https://doi.org/10.25914/5fdb0902607e1(Ukkola et al., 2020).

Author contributions

All authors contributed to the design of the study. WG and MB were responsible for the implementation of PJULES. WG conducted the analyses presented in this paper. WG, SPH, MB, PLG, ICP and SPH all contributed to the interpretation of the analyses. WG and SPH wrote the first draft of the paper, and all authors contributed to the final draft.

Competing interests

The authors declare no competing interests.

Acknowledgements

This work is a contribution to the LEMONTREE (Land Ecosystem Models based On New Theory, obseRvations and ExperimEnts) project, supported by Schmidt Sciences. We thank our colleagues in the wider LEMONTREE team for technical support and discussion of the findings.

Financial Support

This work was supported by Schmidt Sciences.

References

Anav, A., Friedlingstein, P., Beer, C., Ciais, P., Harper, A., Jones, C., Murray-Tortarolo, G., Papale, D., Parazoo, N., Peylin, P., Piao, S., Sitch, S., Viovy, N., Wiltshire, A., and Zhao, M.: Spatio-temporal patterns of terrestrial gross primary production: A review, Rev. Geophys., 53, 785–818, https://doi.org/10.1002/2015RG000483, 2015.

Bassiouni, M., Good, S. P., Still, C. J., and Higgins, C. W.: Plant water uptake thresholds inferred from satellite soil moisture, Geophys. Res. Lett., 47, e2020GL087077, https://doi.org/10.1029/2020GL087077, 2020.

https://doi.org/10.5194/egusphere-2026-2804
Preprint. Discussion started: 28 July 2026

Beer, C., Reichstein, M., Tomelleri, E., Ciais, P., Jung, M., Carvalhais, N., Rödenbeck, C., Arain, M. A., Baldocchi, D., Bonan, G. B., Bondeau, A., Cescatti, A., Lasslop, G., Lindroth, A., Lomas, M., Luyssaert, S., Margolis, H., Oleson, K. W., Roupsard, O., Veenendaal, E., Viovy, N., Williams, C., Woodward, F. I., and Papale, D.: Terrestrial gross carbon dioxide uptake: global distribution and covariation with climate, Science, 329, 834–838, https://doi.org/10.1126/science.1184984, 2010.

Beljaars, A. C. M. and Holtslag, A. A. M.: Flux parameterization over land surfaces for atmospheric models, J. Appl. Meteorol., 30, 327–341, https://doi.org/10.1175/1520-0450(1991)030<0327:FPOLSF>2.0.CO;2, 1991.

Bernacchi, C. J., Singsaas, E. L., Pimentel, C., Portis Jr., A. R., and Long, S. P.: Improved temperature response functions for models of Rubisco-limited photosynthesis, Plant Cell Environ., 24, 253–259, https://doi.org/10.1111/j.1365-3040.2001.00668.x, 2001.

Bernacchi, C. J., Pimentel, C., and Long, S. P.: In vivo temperature response functions of parameters required to model RuBP-limited photosynthesis, Plant Cell Environ., 26, 1419–1430, https://doi.org/10.1046/j.0016-8025.2003.01050.x, 2003.

Best, M. J., Pryor, M., Clark, D. B., Rooney, G. G., Essery, R. L. H., Ménard, C. B., Edwards, J. M., Hendry, M. A., Porson, A., Gedney, N., Mercado, L. M., Sitch, S., Blyth, E., Boucher, O., Cox, P. M., Grimmond, C. S. B., and Harding, R. J.: The Joint UK Land Environment Simulator (JULES), model description – Part 1: Energy and water fluxes, Geosci. Model Dev., 4, 677–699, https://doi.org/10.5194/gmd-4-677-2011, 2011.

Blyth, E. M., Arora, V. K., Clark, D. B., Dadson, S. J., De Kauwe, M. G., Lawrence, D. M., Melton, J. R., Pongratz, J., Turton, R. H., Yoshimura, K., and Yuan, H.: Advances in land surface modelling, Curr. Clim. Change Rep., 7, 45–71, https://doi.org/10.1007/s40641-021-00171-5, 2021.

Burton, C., Betts, R., Cardoso, M., Feldpausch, T. R., Harper, A., Jones, C. D., Kelley, D. I., Robertson, E., and Wiltshire, A.: Representation of fire, land-use change and vegetation dynamics in the Joint UK Land Environment Simulator vn4.9 (JULES), Geosci. Model Dev., 12, 179–193, https://doi.org/10.5194/gmd-12-179-2019, 2019.

https://doi.org/10.5194/egusphere-2026-2804
Preprint. Discussion started: 28 July 2026

830 von Caemmerer, S. and Farquhar, G. D.: Some relationships between the biochemistry of
831 photosynthesis and the gas exchange of leaves, Planta, 153, 376–387,
832 https://doi.org/10.1007/BF00384257, 1981.

833 Calonne, N., Flin, F., Morin, S., Lesaffre, B., Du Roscoat, S. R., and Geindreau, C.: Numerical
834 and experimental investigations of the effective thermal conductivity of snow, Geophys. Res.
835 Lett., 38, L23501, https://doi.org/10.1029/2011GL049234, 2011.

836 Campbell, J. E., Berry, J. A., Seibt, U., Smith, S. J., Montzka, S. A., Launois, T., Belviso, S.,
837 Bopp, L., and Laine, M.: Large historical growth in global terrestrial gross primary production,
838 Nature, 544, 84–87, https://doi.org/10.1038/nature22030, 2017.

839 Canadell, J. G., Monteiro, P. M. S., Costa, M. H., Cunha, L. C. D., Cox, P. M., Eliseev, A. V.,
840 Henson, S., Ishii, M., Jaccard, S., Koven, C., Lohila, A., Patra, P. K., Piao, S., Syampungani,
841 S., Zaehle, S., and Zickfeld, K.: Global carbon and other biogeochemical cycles and feedbacks,
842 in: Climate Change 2021: The Physical Science Basis. Contribution of Working Group I to the
843 Sixth Assessment Report of the Intergovernmental Panel on Climate Change, edited by:
844 Masson-Delmotte, V., Zhai, P., Pirani, A., Connors, S. L., Péan, C., Berger, S., Caud, N., Chen,
845 Y., Goldfarb, L., Gomis, M. I., Huang, M., Leitzell, K., Lonnoy, E., Matthews, J. B. R.,
846 Maycock, T. K., Waterfield, T., Yelekçi, O., Yu, R., and Zhou, B., Cambridge University Press,
847 Cambridge, UK and New York, NY, USA, 673–816,
848 https://doi.org/10.1017/9781009157896.007, 2021.

849 Carter, K. R., Wood, T. E., Reed, S. C., Butts, K. M., and Cavaleri, M. A.: Experimental
850 warming across a tropical forest canopy height gradient reveals minimal photosynthetic and
851 respiratory acclimation, Plant Cell Environ., 44, 2879–2897, https://doi.org/10.1111/pce.14134,
852 2021.

853 Clark, D. B., Mercado, L. M., Sitch, S., Jones, C. D., Gedney, N., Best, M. J., Pryor, M.,
854 Rooney, G. G., Essery, R. L. H., Blyth, E., Boucher, O., Harding, R. J., Huntingford, C., and
855 Cox, P. M.: The Joint UK Land Environment Simulator (JULES), model description – Part 2:
856 Carbon fluxes and vegetation dynamics, Geosci. Model Dev., 4, 701–722,
857 https://doi.org/10.5194/gmd-4-701-2011, 2011.

https://doi.org/10.5194/egusphere-2026-2804
Preprint. Discussion started: 28 July 2026

Collatz, G. J., Ball, J. T., Grivet, C., and Berry, J. A.: Physiological and environmental regulation of stomatal conductance, photosynthesis and transpiration: a model that includes a laminar boundary layer, Agric. For. Meteorol., 54, 107–136, https://doi.org/10.1016/0168-1923(91)90002-8, 1991.

Cox, P. M.: Description of the TRIFFID dynamic global vegetation model, Hadley Centre Technical Note 24, Met Office, Bracknell, UK, 16 pp., 2001.

Cox, P. M., Huntingford, C., and Harding, R. J.: A canopy conductance and photosynthesis model for use in a GCM land surface scheme, J. Hydrol., 212–213, 79–94, https://doi.org/10.1016/S0022-1694(98)00203-0, 1998.

Cox, P. M., Betts, R. A., Bunton, C. B., Essery, R. L. H., Rowntree, P. R., and Smith, J.: The impact of new land surface physics on the GCM simulation of climate and climate sensitivity, Clim. Dyn., 15, 183–203, https://doi.org/10.1007/s003820050276, 1999.

Crous, K. Y.: Plant responses to climate warming: physiological adjustments and implications for plant functioning in a future, warmer world, Am. J. Bot., 106, 1049–1051, https://doi.org/10.1002/ajb2.1329, 2019.

Dyer, A. J.: A review of flux-profile relationships, Boundary-Layer Meteorol, 7, 363–372, https://doi.org/10.1007/BF00240838, 1974.

Drake, J. E., Aspinwall, M. J., Pfautsch, S., Rymer, P. D., Reich, P. B., Smith, R. A., Crous, K. Y., Tissue, D. T., Ghannoum, O., and Tjoelker, M. G.: The capacity to cope with climate warming declines from temperate to tropical latitudes in two widely distributed Eucalyptus species, Glob. Change Biol., 21, 459–472, https://doi.org/10.1111/gcb.12729, 2015.

Dusenge, M. E., Madhavji, S., and Way, D. A.: Contrasting acclimation responses to elevated CO2 and warming between an evergreen and a deciduous boreal conifer, Glob. Change Biol., 26, 3639–3657, https://doi.org/10.1111/gcb.15084, 2020.

Ensminger, I., Sveshnikov, D., Campbell, D. A., Funk, C., Jansson, S., Lloyd, J., Shibistova, O., and Öquist, G.: Intermittent low temperatures constrain spring recovery of photosynthesis in boreal Scots pine forests, Glob. Change Biol., 10, 995–1008, https://doi.org/10.1111/j.1365-2486.2004.00781.x, 2004.

https://doi.org/10.5194/egusphere-2026-2804
Preprint. Discussion started: 28 July 2026

886 Farquhar, G. D., von Caemmerer, S., and Berry, J. A.: A biochemical model of photosynthetic
887 CO2 assimilation in leaves of C3 species, Planta, 149, 78–90,
888 https://doi.org/10.1007/BF00386231, 1980.

889 Fisher, R. A. and Koven, C. D.: Perspectives on the future of land surface models and the
890 challenges of representing complex terrestrial systems, J. Adv. Model. Earth Syst., 12,
891 e2018MS001453, https://doi.org/10.1029/2018MS001453, 2020.

892 Friedlingstein, P., O'Sullivan, M., Jones, M. W., Andrew, R. M., Bakker, D. C. E., Hauck, J.,
893 Landschützer, P., Le Quéré, C., Li, H., Luijkx, I. T., Peters, G. P., Peters, W., Pongratz, J.,
894 Schwingshackl, C., Sitch, S., Canadell, J. G., Ciais, P., et al.: Global Carbon Budget 2025,
895 Earth Syst. Sci. Data Discuss. [preprint], https://doi.org/10.5194/essd-2025-659, in review,
896 2025.

897 Fu, Z., Ciais, P., Makowski, D., Bastos, A., Stoy, P. C., Ibrom, A., Knohl, A., Migliavacca, M.,
898 Cuntz, M., Šigut, L., Peichl, M., Loustau, D., El-Madany, T. S., Buchmann, N., Gharun, M.,
899 Janssens, I., Markwitz, C., Grünwald, T., Rebmann, C., Mölder, M., Varlagin, A., Mammarella,
900 I., Kolari, P., Bernhofer, C., Heliasz, M., Vincke, C., Pitacco, A., Cremonese, E., Foltýnová,
901 L., and Wigneron, J.-P.: Uncovering the critical soil moisture thresholds of plant water stress
902 for European ecosystems, Glob. Change Biol., 28, 2111–2123,
903 https://doi.org/10.1111/gcb.16050, 2022.

904 Fu, Z., Ciais, P., Wigneron, J.-P., Gentine, P., Feldman, A. F., Makowski, D., Viovy, N.,
905 Kemanian, A. R., Goll, D. S., Stoy, P. C., Prentice, I. C., Yakir, D., Liu, L., Ma, H., Li, X.,
906 Huang, Y., Yu, K., Zhu, P., Li, X., Zhu, Z., Lian, J., and Smith, W. K.: Global critical soil
907 moisture thresholds of plant water stress, Nat. Commun., 15, 4826,
908 https://doi.org/10.1038/s41467-024-49244-7, 2024.

909 Gan, W. JULES P-model Site-level Simulations: Model Output, Configuration Files and
910 Analysis Code. Zenodo, 22 May 2026, https://doi.org/10.5281/zenodo.20344326.

911 Gedney, N. and Cox, P. M.: The sensitivity of global climate model simulations to the
912 representation of soil moisture heterogeneity, J. Hydrometeorol., 4, 1265–1275,
913 https://doi.org/10.1175/1525-7541(2003)004<1265:TSOGCM>2.0.CO;2, 2003.

https://doi.org/10.5194/egusphere-2026-2804
Preprint. Discussion started: 28 July 2026

914 Harper, A. B., Cox, P. M., Friedlingstein, P., Wiltshire, A. J., Jones, C. D., Sitch, S., Mercado,
915 L. M., Groenendijk, M., Robertson, E., Kattge, J., Bönisch, G., Atkin, O. K., Bahn, M.,
916 Cornelissen, J., Niinemets, Ü., Onipchenko, V., Peñuelas, J., Poorter, L., Reich, P. B.,
917 Soudzilovskaia, N. A., and van Bodegom, P.: Improved representation of plant functional types
918 and physiology in the Joint UK Land Environment Simulator (JULES v4.2) using plant trait
919 information, Geosci. Model Dev., 9, 2415–2440, https://doi.org/10.5194/gmd-9-2415-2016,
920 2016.

921 Harper, A. B., Wiltshire, A. J., Cox, P. M., Friedlingstein, P., Jones, C. D., Mercado, L. M.,
922 Sitch, S., Williams, K., and Duran-Rojas, C.: Vegetation distribution and terrestrial carbon
923 cycle in a carbon cycle configuration of JULES4.6 with new plant functional types, Geosci.
924 Model Dev., 11, 2857–2873, https://doi.org/10.5194/gmd-11-2857-2018, 2018.

925 Harper, A. B., Williams, K. E., McGuire, P. C., Duran Rojas, M. C., Hemming, D., Verhoef,
926 A., Huntingford, C., Rowland, L., Marthews, T., Breder Eller, C., Mathison, C., Nobrega, R.
927 L. B., Gedney, N., Vidale, P. L., Otu-Larbi, F., Pandey, D., Garrigues, S., Wright, A., Slevin,
928 D., De Kauwe, M. G., Blyth, E., Ardö, J., Black, A., Bonal, D., Buchmann, N., Burban, B.,
929 Fuchs, K., de Grandcourt, A., Mammarella, I., Merbold, L., Montagnani, L., Nouvellon, Y.,
930 Restrepo-Coupe, N., and Wohlfahrt, G.: Improvement of modeling plant responses to low soil
931 moisture in JULESvn4.9 and evaluation against flux tower measurements, Geosci. Model Dev.,
932 14, 3269–3294, https://doi.org/10.5194/gmd-14-3269-2021, 2021.

933 Harrison, S. P., Cramer, W., Franklin, O., Prentice, I. C., Wang, H., Brännström, Å., de Boer,
934 H., Dieckmann, U., Joshi, J., Keenan, T. F., Lavergne, A., Manzoni, S., Mengoli, G.,
935 Morfopoulos, C., Peñuelas, J., Pietsch, S., Rebel, K. T., Ryu, Y., Smith, N. G., Stocker, B. D.,
936 and Wright, I. J.: Eco-evolutionary optimality as a means to improve vegetation and land-
937 surface models, New Phytol., 231, 2125–2141, https://doi.org/10.1111/nph.17558, 2021.

938 Haxeltine, A. and Prentice, I. C.: A general model for the light-use efficiency of primary
939 production, Funct. Ecol., 10, 551–561, https://doi.org/10.2307/2390165, 1996.

940 Jacobs, C. M. J.: Direct impact of atmospheric CO2 enrichment on regional transpiration, PhD
941 thesis, Wageningen Agricultural University, Wageningen, the Netherlands, 179 pp.,
942 https://doi.org/10.18174/206972, 1994.

https://doi.org/10.5194/egusphere-2026-2804
Preprint. Discussion started: 28 July 2026

Jiang, C. and Ryu, Y.: Multi-scale evaluation of global gross primary productivity and evapotranspiration products derived from Breathing Earth System Simulator (BESS), Remote Sens. Environ., 186, 528–547, https://doi.org/10.1016/j.rse.2016.08.030, 2016.

Kattge, J. and Knorr, W.: Temperature acclimation in a biochemical model of photosynthesis: a reanalysis of data from 36 species, Plant Cell Environ., 30, 1176–1190, https://doi.org/10.1111/j.1365-3040.2007.01690.x, 2007.

Kumarathunge, D. P., Medlyn, B. E., Drake, J. E., Tjoelker, M. G., Aspinwall, M. J., Battaglia, M., Cano, F. J., Carter, K. R., Cavaleri, M. A., Cernusak, L. A., Chambers, J. Q., Crous, K. Y., De Kauwe, M. G., Dillaway, D. N., Dreyer, E., Ellsworth, D. S., Ghannoum, O., Han, Q., Hikosaka, K., Jensen, A. M., Kelly, J. W. G., Kruger, E. L., Mercado, L. M., Onoda, Y., Reich, P. B., Rogers, A., Slot, M., Smith, N. G., Tarvainen, L., Tissue, D. T., Togashi, H. F., Tribuzy, E. S., Uddling, J., Vårhammar, A., Wallin, G., Warren, J. M., and Way, D. A.: Acclimation and adaptation components of the temperature dependence of plant photosynthesis at the global scale, New Phytol., 222, 768–784, https://doi.org/10.1111/nph.15668, 2019.

Lawrence, D. M., Fisher, R. A., Koven, C. D., Oleson, K. W., Swenson, S. C., Bonan, G., Collier, N., Ghimire, B., van Kampenhout, L., Kennedy, D., Kluzek, E., Lawrence, P. J., Li, F., Li, H., Lombardozzi, D., Riley, W. J., Sacks, W. J., Shi, M., Vertenstein, M., Wieder, W. R., Xu, C., Ali, A. A., Badger, A. M., Bisht, G., van den Broeke, M., Brunke, M. A., Burns, S. P., Buzan, J., Clark, M., Craig, A., Dahlin, K., Drewniak, B., Fisher, J. B., Flanner, M., Fox, A. M., Gentine, P., Hoffman, F., Keppel-Aleks, G., Knox, R., Kumar, S., Lenaerts, J., Leung, L. R., Lipscomb, W. H., Lu, Y., Pandey, A., Pelletier, J. D., Perket, J., Randerson, J. T., Ricciuto, D. M., Sanderson, B. M., Slater, A., Subin, Z. M., Tang, J., Thomas, R. Q., Val Martin, M., and Zeng, X.: The Community Land Model Version 5: description of new features, benchmarking, and impact of forcing uncertainty, J. Adv. Model. Earth Syst., 11, 4245–4287, https://doi.org/10.1029/2018MS001583, 2019.

Luo, X., Zhou, H., Satriawan, T. W., Tian, J., Zhao, R., Keenan, T. F., Griffith, D. M., Sitch, S., Smith, N. G., and Still, C. J.: Mapping the global distribution of C4 vegetation using observations and optimality theory, Nat. Commun., 15, 1219, https://doi.org/10.1038/s41467-024-45606-3, 2024.

https://doi.org/10.5194/egusphere-2026-2804
Preprint. Discussion started: 28 July 2026

Luo, Y., Gessler, A., D'Odorico, P., Hufkens, K., and Stocker, B. D.: Quantifying effects of cold acclimation and delayed springtime photosynthesis resumption in northern ecosystems, New Phytol., 240, 984–1002, https://doi.org/10.1111/nph.19208, 2023.

Maire, V., Martre, P., Kattge, J., Gastal, F., Esser, G., Fontaine, S., and Soussana, J.-F.: The coordination of leaf photosynthesis links C and N fluxes in C3 plant species, PLoS ONE, 7, e38345, https://doi.org/10.1371/journal.pone.0038345, 2012.

Mäkelä, A., Hari, P., Berninger, F., Hänninen, H., and Nikinmaa, E.: Acclimation of photosynthetic capacity in Scots pine to the annual cycle of temperature, Tree Physiol., 24, 369–376, https://doi.org/10.1093/treephys/24.4.369, 2004.

Mäkelä, A., Pulkkinen, M., Kolari, P., Lagergren, F., Berbigier, P., Lindroth, A., Loustau, D., Nikinmaa, E., Vesala, T., and Hari, P.: Developing an empirical model of stand GPP with the LUE approach: analysis of eddy covariance data at five contrasting conifer sites in Europe, Glob. Change Biol., 14, 92–108, https://doi.org/10.1111/j.1365-2486.2007.01463.x, 2008.

Mengoli, G., Agustí-Panareda, A., Boussetta, S., Harrison, S. P., Trotta, C., and Prentice, I. C.: Ecosystem photosynthesis in land-surface models: a first-principles approach incorporating acclimation, J. Adv. Model. Earth Syst., 14, e2021MS002767, https://doi.org/10.1029/2021MS002767, 2022.

Miralles, D. G., Bonte, O., Koppa, A., Baez-Villanueva, O. M., Tronquo, E., Zhong, F., Beck, H. E., Hulsman, P., Dorigo, W., Verhoest, N. E. C., and Haghdoost, S.: GLEAM4: global land evaporation and soil moisture dataset at 0.1° resolution from 1980 to near present, Sci. Data, 12, 416, https://doi.org/10.1038/s41597-025-04610-y, 2025.

Morton, D. C., Nagol, J., Carabajal, C. C., Rosette, J., Palace, M., Cook, B. D., Vermote, E. F., Harding, D. J., and North, P. R. J.: Amazon forests maintain consistent canopy structure and greenness during the dry season, Nature, 506, 221–224, https://doi.org/10.1038/nature13006, 2014.

Oliver, R. J., Mercado, L. M., Clark, D. B., Huntingford, C., Taylor, C. M., Vidale, P. L., McGuire, P. C., Todt, M., Folwell, S., Shamsudheen Semeena, V., and Medlyn, B. E.: Improved representation of plant physiology in the JULES-vn5.6 land surface model:

https://doi.org/10.5194/egusphere-2026-2804
Preprint. Discussion started: 28 July 2026

photosynthesis, stomatal conductance and thermal acclimation, Geosci. Model Dev., 15, 5567–5592, https://doi.org/10.5194/gmd-15-5567-2022, 2022.

Oliver, R. J., Mercado, L. M., Medlyn, B. E., Harris, P. P., and Clark, D. B.: Contrasting impacts of acclimation and adaptation of photosynthetic capacity to temperature and CO2 across biomes, Global Biogeochem. Cy., 39, e2024GB008398, https://doi.org/10.1029/2024GB008398, 2025.

Pedregosa, F., Varoquaux, G., Gramfort, A., Michel, V., Thirion, B., Grisel, O., Blondel, M., Prettenhofer, P., Weiss, R., Dubourg, V., Vanderplas, J., Passos, A., Cournapeau, D., Brucher, M., Perrot, M., and Duchesnay, E.: Scikit-learn: machine learning in Python, J. Mach. Learn. Res., 12, 2825–2830, 2011.

Prentice, I. C., Dong, N., Gleason, S. M., Maire, V., and Wright, I. J.: Balancing the costs of carbon gain and water transport: testing a new theoretical framework for plant functional ecology, Ecol. Lett., 17, 82–91, https://doi.org/10.1111/ele.12211, 2014.

Raoult, N., Douglas, N., MacBean, N., Kolassa, J., Quaife, T., Roberts, A. G., Fisher, R., Fer, I., Bacour, C., Dagon, K., Hawkins, L., Carvalhais, N., Cooper, E., Dietze, M. C., Gentine, P., Kaminski, T., Kennedy, D., Liddy, H. M., Moore, D. J. P., Peylin, P., Pinnington, E., Sanderson, B., Scholze, M., Seiler, C., Smallman, T. L., Vergopolan, N., Viskari, T., Williams, M., and Zobitz, J.: Parameter estimation in land surface models: challenges and opportunities with data assimilation and machine learning, J. Adv. Model. Earth Syst., 17, e2024MS004733, https://doi.org/10.1029/2024MS004733, 2025.

Reich, P. B., Sendall, K. M., Stefanski, A., Rich, R. L., Hobbie, S. E., and Montgomery, R. A.: Effects of climate warming on photosynthesis in boreal tree species depend on soil moisture, Nature, 562, 263–267, https://doi.org/10.1038/s41586-018-0582-4, 2018.

Rogers, A., Medlyn, B. E., Dukes, J. S., Bonan, G., von Caemmerer, S., Dietze, M. C., Kattge, J., Leakey, A. D. B., Mercado, L. M., Niinemets, Ü., Prentice, I. C., Serbin, S. P., Sitch, S., Way, D. A., and Zaehle, S.: A roadmap for improving the representation of photosynthesis in Earth system models, New Phytol., 213, 22–42, https://doi.org/10.1111/nph.14283, 2017.

Ruehr, S., Keenan, T. F., Williams, C., Zhou, Y., Lu, X., Bastos, A., Canadell, J. G., Prentice, I. C., Sitch, S., and Terrer, C.: Publisher Correction: Evidence and attribution of the enhanced

https://doi.org/10.5194/egusphere-2026-2804
Preprint. Discussion started: 28 July 2026

land carbon sink, Nat. Rev. Earth Environ., 4, 864, https://doi.org/10.1038/s43017-023-00503-z, 2023.

Saleska, S. R., Miller, S. D., Matross, D. M., Goulden, M. L., Wofsy, S. C., da Rocha, H. R., de Camargo, P. B., Crill, P., Daube, B. C., de Freitas, H. C., Hutyra, L., Keller, M., Kirchhoff, V., Menton, M., Munger, J. W., Pyle, E. H., Rice, A. H., and Silva, H.: Carbon in Amazon forests: unexpected seasonal fluxes and disturbance-induced losses, Science, 302, 1554–1557, https://doi.org/10.1126/science.1091165, 2003.

Scafaro, A. P., Xiang, S., Long, B. M., Bahar, N. H. A., Weerasinghe, L. K., Creek, D., Evans, J. R., Reich, P. B., and Atkin, O. K.: Strong thermal acclimation of photosynthesis in tropical and temperate wet-forest tree species: the importance of altered Rubisco content, Glob. Change Biol., 23, 2783–2800, https://doi.org/10.1111/gcb.13566, 2017.

Sellar, A. A., Jones, C. G., Mulcahy, J. P., Tang, Y., Yool, A., Wiltshire, A., O'Connor, F. M., Stringer, M., Hill, R., Palmieri, J., Woodward, S., de Mora, L., Kuhlbrodt, T., Rumbold, S. T., Kelley, D. I., Ellis, R., Johnson, C. E., Walton, J., Abraham, N. L., Andrews, M. B., Andrews, T., Archibald, A. T., Berthou, S., Burke, E., Blockley, E., Carslaw, K., Dalvi, M., Edwards, J., Folberth, G. A., Gedney, N., Griffiths, P. T., Harper, A. B., Hendry, M. A., Hewitt, A. J., Johnson, B., Jones, A., Jones, C. D., Keeble, J., Liddicoat, S., Morgenstern, O., Parker, R. J., Predoi, V., Robertson, E., Siahaan, A., Smith, R. S., Swaminathan, R., Woodhouse, M. T., Zeng, G., and Zerroukat, M.: UKESM1: description and evaluation of the U.K. Earth System Model, J. Adv. Model. Earth Syst., 11, 4513–4558, https://doi.org/10.1029/2019MS001739, 2019.

Sellers, P. J.: Canopy reflectance, photosynthesis and transpiration, Int. J. Remote Sens., 6, 1335–1372, https://doi.org/10.1080/01431168508948283, 1985.

Smith, N. G. and Dukes, J. S.: Short-term acclimation to warmer temperatures accelerates leaf carbon exchange processes across plant types, Glob. Change Biol., 23, 4840–4853, https://doi.org/10.1111/gcb.13735, 2017.

Still, C. J., Berry, J. A., Collatz, G. J., and DeFries, R. S.: Global distribution of C3 and C4 vegetation: carbon cycle implications, Global Biogeochem. Cy., 17, 1006, https://doi.org/10.1029/2001GB001807, 2003.

https://doi.org/10.5194/egusphere-2026-2804
Preprint. Discussion started: 28 July 2026

Stocker, B. D., Zscheischler, J., Keenan, T. F., Prentice, I. C., Peñuelas, J., and Seneviratne, S. I.: Quantifying soil moisture impacts on light use efficiency across biomes, New Phytol., 218, 1430–1449, https://doi.org/10.1111/nph.15123, 2018.

Stocker, B. D., Wang, H., Smith, N. G., Harrison, S. P., Keenan, T. F., Sandoval, D., Davis, T., and Prentice, I. C.: P-model v1.0: an optimality-based light use efficiency model for simulating ecosystem gross primary production, Geosci. Model Dev., 13, 1545–1581, https://doi.org/10.5194/gmd-13-1545-2020, 2020.

Stocker, B. D., Dong, N., Perkowski, E. A., Schneider, P. D., Xu, H., De Boer, H. J., Rebel, K. T., Smith, N. G., Van Sundert, K., Wang, H., Jones, S. E., Prentice, I. C., and Harrison, S. P.: Empirical evidence and theoretical understanding of ecosystem carbon and nitrogen cycle interactions, New Phytol., 245, 49–68, https://doi.org/10.1111/nph.20178, 2025.

Tanja, S., Berninger, F., Vesala, T., Markkanen, T., Hari, P., Mäkelä, A., Ilvesniemi, H., Hänninen, H., Nikinmaa, E., Huttula, T., Laurila, T., Aurela, M., Grelle, A., Lindroth, A., Arneth, A., Shibistova, O., and Lloyd, J.: Air temperature triggers the recovery of evergreen boreal forest photosynthesis in spring, Glob. Change Biol., 9, 1410–1426, https://doi.org/10.1046/j.1365-2486.2003.00597.x, 2003.

Ukkola, A. M., Abramowitz, G., and De Kauwe, M. G.: A flux tower dataset tailored for land model evaluation, Earth Syst. Sci. Data, 14, 449–461, https://doi.org/10.5194/essd-14-449-2022, 2022.

Van den Hoof, C., Vidale, P. L., Verhoef, A., and Vincke, C.: Improved evaporative flux partitioning and carbon flux in the land surface model JULES: impact on the simulation of land surface processes in temperate Europe, Agric. For. Meteorol., 181, 108–124, https://doi.org/10.1016/j.agrformet.2013.07.011, 2013.

Verhoeven, A.: Sustained energy dissipation in winter evergreens, New Phytol., 201, 57–65, https://doi.org/10.1111/nph.12466, 2014.

Wang, H., Prentice, I. C., Keenan, T. F., Davis, T. W., Wright, I. J., Cornwell, W. K., Evans, B. J., and Peng, C.: Towards a universal model for carbon dioxide uptake by plants, Nat. Plants, 3, 734–741, https://doi.org/10.1038/s41477-017-0006-8, 2017.

https://doi.org/10.5194/egusphere-2026-2804
Preprint. Discussion started: 28 July 2026

1086 Way, D. A. and Yamori, W.: Thermal acclimation of photosynthesis: on the importance of
1087 adjusting our definitions and accounting for thermal acclimation of respiration, Photosynth.
1088 Res., 119, 89–100, https://doi.org/10.1007/s11120-013-9873-7, 2014.

1089 Williams, K. D., Copsey, D., Blockley, E. W., Bodas-Salcedo, A., Calvert, D., Comer, R.,
1090 Davis, P., Graham, T., Hewitt, H. T., Hill, R., Hyder, P., Ineson, S., Johns, T. C., Keen, A. B.,
1091 Lee, R. W., Megann, A., Milton, S. F., Rae, J. G. L., Roberts, M. J., Scaife, A. A., Schiemann,
1092 R., Storkey, D., Thorpe, L., Watterson, I. G., Walters, D. N., West, A., Wood, R. A., Woollings,
1093 T., and Xavier, P. K.: The Met Office Global Coupled Model 3.0 and 3.1 (GC3.0 and GC3.1)
1094 configurations, J. Adv. Model. Earth Syst., 10, 357–380,
1095 https://doi.org/10.1002/2017MS001115, 2018.

1096 Wiltshire, A. J., Duran Rojas, M. C., Edwards, J. M., Gedney, N., Harper, A. B., Hartley, A. J.,
1097 Hendry, M. A., Robertson, E., and Smout-Day, K.: JULES-GL7: the Global Land configuration
1098 of the Joint UK Land Environment Simulator version 7.0 and 7.2, Geosci. Model Dev., 13,
1099 483–505, https://doi.org/10.5194/gmd-13-483-2020, 2020.

1100 Wiltshire, A. J., Burke, E. J., Chadburn, S. E., Jones, C. D., Cox, P. M., Davies-Barnard, T.,
1101 Friedlingstein, P., Harper, A. B., Liddicoat, S., Sitch, S., and Zaehle, S.: JULES-CN: a coupled
1102 terrestrial carbon–nitrogen scheme (JULES vn5.1), Geosci. Model Dev., 14, 2161–2186,
1103 https://doi.org/10.5194/gmd-14-2161-2021, 2021.

1104 Wright, I. J., Reich, P. B., and Westoby, M.: Least-cost input mixtures of water and nitrogen
1105 for photosynthesis, Am. Nat., 161, 98–111, https://doi.org/10.1086/344920, 2003.

1106 Yamori, W., Hikosaka, K., and Way, D. A.: Temperature response of photosynthesis in C3,
1107 C4, and CAM plants: temperature acclimation and temperature adaptation, Photosynth. Res.,
1108 119, 101–117, https://doi.org/10.1007/s11120-013-9874-6, 2013.

1109 Zhou, B., Cai, W., Zhu, Z., Wang, H., Harrison, S. P., and Prentice, I. C.: A general model for
1110 the seasonal to decadal dynamics of leaf area, Glob. Change Biol., 31, e70125,
1111 https://doi.org/10.1111/gcb.70125, 2025.

1112